Global Biogeochemical Cycles

RESEARCH ARTICLE
10.1029/2020GB006704

Gelatinous Zooplankton-Mediated Carbon Flows in the Global Oceans: A Data-Driven Modeling Study

Jessica Y. Luo[1], Robert H. Condon[2], Charles A. Stock[1], Carlos M. Duarte[3], Cathy H. Lucas[4], Kylie A. Pitt[5], and Robert K. Cowen[6]

[1]NOAA Geophysical Fluid Dynamics Laboratory, Princeton University Forrestal Campus, Princeton, NJ, USA, [2]Young Scientist Academy, Wilmington, NC, USA, [3]Red Sea Research Center (RSRC), King Abdullah University of Science and Technology (KAUST), Thuwal, Saudi Arabia, [4]National Oceanography Centre Southampton, University of Southampton, Waterfront Campus, Southampton, UK, [5]Australian Rivers Institute and School of Environment and Science, Griffith University, Gold Coast Campus, Gold Coast, Australia, [6]Hatfield Marine Science Center, Oregon State University, Newport, OR, USA

Key Points:
- GZ consume a substantial fraction of plankton production, resulting in large export fluxes at 100 m and fast transfer efficiencies to depth
- While the model has a large uncertainty range in GZ-associated fluxes, even values at the low end of the range are globally significant
- Jelly-falls are likely unaccounted for in current estimates of POC flux and may increase global seafloor flux by 8–35% if included

Supporting Information:
- Supporting Information S1

Correspondence to:
J. Y. Luo,
jessica.luo@noaa.gov

Citation:
Luo, J. Y., Condon, R. H., Stock, C. A., Duarte, C. M., Lucas, C. H., Pitt, K. A., & Cowen, R. K. (2020). Gelatinous zooplankton-mediated carbon flows in the global oceans: A data-driven modeling study. *Global Biogeochemical Cycles*, *34*, e2020GB006704. https://doi.org/10.1029/2020GB006704

Received 13 JUN 2020
Accepted 18 AUG 2020
Accepted article online 26 AUG 2020

Abstract Among marine organisms, gelatinous zooplankton (GZ; cnidarians, ctenophores, and pelagic tunicates) are unique in their energetic efficiency, as the gelatinous body plan allows them to process and assimilate high proportions of oceanic carbon. Upon death, their body shape facilitates rapid sinking through the water column, resulting in carcass depositions on the seafloor ("jelly-falls"). GZ are thought to be important components of the biological pump, but their overall contribution to global carbon fluxes remains unknown. Using a data-driven, three-dimensional, carbon cycle model resolved to a 1° global grid, with a Monte Carlo uncertainty analysis, we estimate that GZ consumed 7.9–13 Pg C y^{-1} in phytoplankton and zooplankton, resulting in a net production of 3.9–5.8 Pg C y^{-1} in the upper ocean (top 200 m), with the largest fluxes from pelagic tunicates. Non-predation mortality (carcasses) comprised 25% of GZ production, and combined with the much greater fecal matter flux, total GZ particulate organic carbon (POC) export at 100 m was 1.6–5.2 Pg C y^{-1}, equivalent to 32–40% of the global POC export. The fast sinking GZ export resulted in a high transfer efficiency (T_{eff}) of 38–62% to 1,000 m and 25–40% to the seafloor. Finally, jelly-falls at depths >50 m are likely unaccounted for in current POC flux estimates and could increase benthic POC flux by 8–35%. The significant magnitude of and distinct sinking properties of GZ fluxes support a critical yet underrecognized role of GZ carcasses and fecal matter to the biological pump and air-sea carbon balance.

Plain Language Summary Marine ecosystems play a critical role in the global carbon cycle through food web regulation of air-sea carbon fluxes and the transfer of organic carbon from the upper oceans to the deep sea. The carcasses of gelatinous zooplankton (GZ), which include jellyfish and salps, have been found in mass seafloor depositions ("jelly-falls") in many locations. These jelly-falls are thought to be a fast mechanism for carbon sequestration, yet no global studies on their overall impact have been done. Using a database of GZ observations, we suggest that the inclusion of previously unaccounted for GZ carbon in seafloor carbon deposition could increase current estimates by 8–35%. This previously unconsidered flux represents a substantial amount of carbon sequestered in the deep sea.

1. Introduction

The gelatinous zooplankton (GZ) are a functionally and morphologically diverse group of organisms comprising the cnidarians, ctenophores, and pelagic tunicates, common throughout the world's oceans and exhibiting boom-and-bust population dynamics (Lilley et al., 2011; Lucas et al., 2014; Purcell, 2012). They have been prevalent components of ocean ecosystems for over 500 million years, as fossil records show mass deposition events extending to the late Cambrianera (Hagadorn et al., 2002). Recent studies have identified some of the mechanisms underlying GZ success. These include a body plan that has high water and low carbon content and a set of unique physiological and reproductive traits that allow them to thrive in low-nutrient conditions while rapidly exploiting food increases (Acuña, 2001; Acuña et al., 2011; Lucas & Dawson, 2014; Pitt et al., 2013). However, upon depletion of food resources, the bloom population often busts, resulting in GZ mass mortality events, also known as "jelly-falls" (e.g., Billett et al., 2006).

Field observations of mass seafloor depositions of jellyfish carcasses often find that they are fully intact with low degradation (Billett et al., 2006; Sweetman & Chapman, 2011). Combined with lab measurements of GZ sinking rates (Lebrato, Mendes, et al., 2013), there is increasing evidence that jelly-falls may act as a fast export mechanism for carbon to the deep sea and play an important role within the marine biological pump (Lebrato et al., 2019; Lebrato & Jones, 2009; Steinberg & Landry, 2017; Sweetman & Chapman, 2015). For instance, one 2-day jelly-fall event in the Arabian Sea produced over an order of magnitude more particulate organic carbon (POC) flux to the benthos than annual fluxes measured by sediment traps, which do not typically capture jelly-falls (Billett et al., 2006). However, since GZ have only been included in a few regional (Henschke et al., 2018; Heymans & Baird, 2000; Stone & Steinberg, 2016; Vasas et al., 2007) but no global biogeochemical models, an understanding of the global impact of these events, and other GZ-associated fluxes (e.g., fecal production), on carbon export is lacking. Most recently, Lebrato et al. (2019) used the biomass estimates from Lucas et al. (2014) to estimate the impact of GZ on the transfer efficiency (T_{eff}) of the biological pump if the annual GZ standing stock were to sink with observed GZ sinking rates (Lebrato, Mendes, et al., 2013). However, a key limitation is that Lebrato et al. (2019) did not account for the high productivity and fast turnover rates of the GZ population, which may result in an annual net production many times greater than standing stock biomass. In our present study, we combine a model of GZ biological rate processes with a carbon remineralization model to estimate global GZ biomass production, POC production, and POC fluxes at depth.

Our present study builds on the work of the Jellyfish Database Initiative (JeDI) project, which is a synthesis effort focused on compiling data on GZ spatial distributions (Lucas et al., 2014), temporal fluctuations (Condon et al., 2013), and physiological rate processes (Pitt et al., 2013). JeDI data are made available in an open-source repository (Condon et al., 2015). In this study, we update and revise the previous estimate of GZ standing stock carbon biomass (Lucas et al., 2014) with additional data from JeDI, KRILLBASE (Atkinson et al., 2017), and other sources, as well as compile carbon-based physiological rate parameters for additional GZ taxa not covered by Pitt et al. (2013). Using these updated data, we then develop a data-driven, carbon cycle model for GZ, aimed at understanding the contribution of GZ-mediated carbon to the global marine biological pump.

2. Methods

2.1. Biomass Estimates

GZ carbon biomass was estimated for the three main taxonomic groups (cnidarians, ctenophores, and pelagic tunicates) using 80,517 records of upper ocean GZ individual biomass and numeric density (# individuals m^{-3}), primarily from JeDI database (Condon et al., 2015), and pulled into a vertically integrated annual mean. Lucas et al. (2014, hereafter L14) converted the JeDI biomass records from their original measurement form (e.g., length, wet weight) to carbon (C) biomass using taxa-specific relationships (Lucas et al., 2011) and mapped these onto a 1° latitude/longitude grid. We excluded appendicularians, as they were inconsistently and extremely undersampled in most GZ surveys. Also excluded were 40 anomalously high biomass records from the central North Pacific; these were historic records from the NOAA COPEPOD data set (Moriarty & O'Brien, 2013) that exceeded the mean global density by over two standard deviations.

Additions to the data set made for this study were 1,480 cnidarian records from the northern California Current (Brodeur et al., 2014) and Gulf of Mexico (Robinson et al., 2015) and 891 salp records from the Bermuda Atlantic Time Series (BATS; Stone & Steinberg, 2014) and Western Antarctic Peninsula (WAP; Steinberg et al., 2015). Finally, 9,357 salp records from the Southern Ocean, excluding those already included from WAP, from KRILLBASE (Atkinson et al., 2017) were added, which greatly enhanced the spatial coverage in the Southern Ocean. Biometric conversions to C biomass for the additional data were done for cnidarians (using data for *Chrysaora fuscescens*, Shenker, 1985, and *Aurelia aurita*, Pitt et al., 2013) and salps (Madin & Deibel, 1998). Note that in the original L14 data set, biometric conversions were applied according to the closest related species at the family or class level. Individual records were mapped onto a 1° grid using the geometric mean, following L14. All data were then averaged temporally (month, then year) for a characteristic magnitude. The additions represented 1,564 new 1° grid cells and a 52% increase in spatial coverage relative to L14.

To estimate the global mean biomass, GZ data were aggregated by biome. We designated three major ocean biomes: (1) low chlorophyll (LC), (2) high chlorophyll seasonally stratified (HCSS), and (3) high chlorophyll permanently stratified (HCPS), and a fourth biome for coastal waters <200-m depth. The ocean biomes are consistent with those defined by Banse (1992) to differentiate subtropical gyres, high-latitude oceans with deep winter mixing, and equatorial upwelling zones. A single coastal biome (bottom depth <200 m) was included to account for cnidarian medusae that have a benthic life history stage for asexual reproduction and have population dynamics distinct from pelagic, holoplanktonic species. To define the biomes, we used a combination of satellite chlorophyll from SeaWiFS (1997–2010 mission mean), observational climatology of mixed layer depth (de Boyer Montégut et al., 2004), and bottom depth from the World Ocean Atlas (WOA13v2; for consistency with the rest of the model; see Figure S1 for biome maps and details). Since the GZ biomass was log-normally distributed, the geometric mean was used to determine average values for GZ biomass estimates per biome. An area-weighted sum of the biome-specific GZ biomass then provided the estimate of the global total, reflecting a multidecadal mean magnitude.

Biomass variation around the multidecadal mean was extracted from Condon et al. (2013), which estimated the GZ biomass oscillations since the 1940s, using a method that combined historical, qualitative (presence/absence) biomass reports with more recent, quantitative assessments to generate a standardized index value. These values represent an estimate of temporal variance (σ^2) around a long-term mean, which were 36.5% for cnidarians, 34.4% for ctenophores, and 18.1% for tunicates (Condon et al., 2013). We used these percentages to calculate biomass standard deviation (σ), for setting up a high biomass ($+1\sigma$), low biomass (-1σ), and baseline model cases.

2.2. Estimation of GZ-Associated Carbon Fluxes

GZ-associated carbon fluxes are estimated by integrating the biomass data above with a bioenergetics model to estimate upper ocean fluxes and a particle sinking and remineralization model to estimate fluxes to depth (Lebrato et al., 2011). Physical and biogeochemical fields required for the bioenergetics and export calculations are provided by a combination of global data products and a biogeochemical model that captures plankton food web dynamics across the biomes enlisted herein (Stock et al., 2014). To derive global estimates, fluxes are calculated on the 1° grid, before averaging across biomes as described for GZ biomass above. A Monte Carlo (MC) parameter uncertainty approach, together with the three biomass cases described above, is used to assess uncertainty in estimated fluxes. The subsections below describe the model inputs (section 2.2.1), the bioenergetics calculations used for the upper ocean biology (section 2.2.2), the export submodel (section 2.2.3), and the MC uncertainty estimation (section 2.2.4).

2.2.1. Model Inputs

The present model is a data-driven mechanistic model, with the primary input being the GZ observational data set (section 2.1). We assumed that these observations represented the GZ annual standing stock biomass, which formed the basis of an upper ocean bioenergetics submodel (section 2.2.2). We ran the full model under three different biomass conditions as described above (section 2.1). The bioenergetics model had additional inputs of sea surface temperature (SST) and annual net primary and secondary production. For SST, we used the 1971–2000 long-term mean SST from the NOAA Optimum Interpolation Sea Surface Temperature (OISST) v2 data set (Reynolds et al., 2002). Primary and secondary production (mg C m^{-2} y^{-1}, integrated over the top meter) were derived from outputs of the NOAA-GFDL Carbon, Ocean Biogeochemistry, and Lower Trophics (COBALT v.1) model (Stock et al., 2014), a marine biogeochemical ecosystem model that resolves multiple nutrient cycles and contains an ecosystem representation with three phytoplankton (small/pico-plankton, diazotrophs, and large phytoplankton), heterotrophic bacteria, and three zooplankton. The zooplankton were separated by size classes (small: <200 μm, medium: 200 μm to 2 mm, large: 2–20 mm). Medium and large zooplankton are parameterized as small crustacean copepods and large copepods/krill, respectively. The simulated patterns of plankton food web productivity from COBALT are consistent with large-scale patterns inferred from in situ, laboratory, and satellite observations (Stock et al., 2014), including chlorophyll concentrations, primary production, and zooplankton biomass and production most critical to the GZ bioenergetics model. All inputs to the present model were in a 1° global resolution.

Results from the upper ocean bioenergetics model fed into the export model (section 2.2.3), which calculates the depth- and temperature-dependent biomass remineralization of GZ export in a set of 1-D columns. For

Table 1
List of Variables, Descriptions, and Units Used in the Model

Variable	Description	Equation or value (definition)	Units	Used in MC
AE	Assimilation efficiency		Unitless	X
b	Individual GZ biomass		g C indiv.$^{-1}$	
B	GZ biomass	$B = n * b$	g C m^{-3}	
c_T	Temperature constant		Unitless	X
CR	Clearance rate	Equation 4	m^3 indiv.$^{-1}$ y^{-1}	
dB/dt	GZ annual production rate	Equation 1	g C m^{-3} y^{-1}	
E	Exudation rate	$E = f_E * P$	g C indiv.$^{-1}$ y^{-1}	
E_a	Activation energy	0.65	eV	
Eg	Egestion rate	Equation 2	g C m^{-3} y^{-1}	
ESD	Equivalent spherical diameter		cm indiv.$^{-1}$	
f_E	Fraction of production to exudation		Unitless	X
f_{RL}	Fraction of production to reproductive loss		Unitless	X
f_{Pr}	Fraction of production to predation		Unitless	X
I	Ingestion rate	Equation 3	g C indiv.$^{-1}$ y^{-1}	
k	Boltzmann constant	8.617×10^5	eV K^{-1}	
n	GZ numeric density		Indiv. m^{-3}	
P	Production rate	$P = (AE * I) - R$	g C indiv.$^{-1}$ y^{-1}	
Pr	Predation rate	$Pr = f_{Pr} * P$	g C indiv.$^{-1}$ y^{-1}	
pb	Prey biomass		g C m^{-3}	
R	Respiration rate	Equations 5 and 6	g C indiv.$^{-1}$ y^{-1}	
RL	Reproductive loss rate	$RL = f_{RL} * P$	g C indiv.$^{-1}$ y^{-1}	
SST	Sea surface temperature		Degrees Kelvin	
T	Temperature at average depth	$T = c_T * SST$	Degrees Kelvin	
β_{CR1}	Clearance rate allometric scaling slope		Unitless	X
β_{CR2}	Clearance rate allometric scaling intercept		m^3 (g C)$^{-1}$ y^{-1}	X
β_{ESD1}	ESD—biomass scaling slope		Unitless	X
β_{ESD2}	ESD—biomass scaling intercept		cm (g C)$^{-1}$	X
β_{R1_ch}	Resp. rate scaling slope (tunicate)		Unitless	X
$\beta_{R1\_cn,ct}$	Resp. rate scaling slope (cnid., cten.)		Unitless	X

Note. The generalized allometric scaling equations are $y = mx^n$, which can also be represented as $\log(y) = n * \log(x) + \log(m)$. Here, the β_2 (allometric scaling intercept) terms are the $\log(m)$ terms and technically are unitless. For simplicity, we list the units of m as the units of the β_2 terms.

inputs, we used ocean temperatures from the World Ocean Atlas (WOA) 2013v2, which provided long-term mean (1955–2012) temperatures within 102 depth bins (from surface to 5,500 m; Locarnini et al., 2013), also in a 1° grid.

2.2.2. Upper Ocean Bioenergetics Submodel

The bioenergetics model represents biologically mediated carbon fluxes through the three main GZ groups: cnidarians, ctenophores, and pelagic tunicates (salps), in the upper 200 m. The three GZ groups were modeled separately and were mostly non-interacting, except via food limitation from the shared zooplankton prey of cnidarians and ctenophores. We used allometric relationships to model physiological processes, and using the carbon biomass and numeric density estimates (section 2.1), we modeled an average-sized individual from each GZ group per grid cell. As the target quantity from the bioenergetics submodel was POC export, we solved for POC production as the residual of the ingestion minus the routing to other carbon pools via physiological processes (respiration, reproductive loss, etc.).

The generalized equation for GZ production (dB/dt, g C m^{-3} y^{-1}) is

$$\frac{dB}{dt} = n\left((AE \times I) - R - RL - E - Pr\right) - M \quad (1)$$

where n is the number of individuals, AE is assimilation efficiency, I is prey ingestion, R is respiration, RL is loss due to reproduction, E is exudation, Pr is predation by higher trophic levels, and M is loss due to senescence, or non-predatory mortality (for a full list of abbreviations and units, see Table 1). The non-assimilated material is released as fecal matter, or egestion (Eg):

$$Eg = n((1 - AE) \times I) \quad (2)$$

Together, the egestion and non-predatory mortality terms represent the POC production by GZ. The remainder of this section details the parameterization of each term in Equation 1.

The amount of carbon assimilated into an organism is a function of its assimilation efficiency (*AE*) and ingestion, which is in turn a product of its clearance rate (*CR*) and the available prey biomass (*pb*) (Equation 3):

$$I = CR \times pb \quad (3)$$

CR was calculated using allometric relationships based on a combination of temperature and body size (Equation 4) following the metabolic theory of ecology (MTE; Brown et al., 2004).

$$\log(CR) = (\beta_{CR1} log(b) + \beta_{CR2})\, e^{\left(-E_a/kT\right)} \quad (4)$$

For cnidarians and ctenophores, we used published relationships between clearance rate and carbon biomass to constrain the MC parameters (Acuña et al., 2011). Equivalent relationships for pelagic tunicates (salps) were not available and thus were derived from the experimental literature (see Tables S1 and S2).

We used annual mean, top 200-m phytoplankton and zooplankton biomass (g C m^{-3}) from the GFDL-COBALT v.1 model (Stock et al., 2014), as the prey pool (*pb*). For cnidarians and ctenophores, the prey field was medium and large zooplankton. For tunicates, the prey field was small phytoplankton and a fraction of large phytoplankton (50%), diazotrophs (50%), and microzooplankton (33%). The large phytoplankton size classes (including diazotrophs, which are parameterized as *Trichodesmium* in COBALT) and microzooplankton were less available for tunicate feeding due to their lower affinity for and/or filtering efficiency of large particles (Sutherland et al., 2010). Since this is an "offline" model, there is a potential for simulations associated with a given set of parameters to try and consume more food than is available. We thus only consider those MC sets for which the total consumption is lower than the total production of the prey groups (see section 2.2.4). We also recognize that in a fully coupled (i.e., online) model, consumption of one trophic level (e.g., microzooplankton) would reduce production rates for other trophic levels (e.g., small mesozooplankton). A full exploration of these feedbacks is left to future work.

Respiration (*R*) was also determined using allometric relationships between physiological rate, temperature, and body size (Equations 5 and 6).

$$\log\left(R_{cn,\,ct}\right) = \left(\beta_{R1\_cn,\,ct} log(ESD) + \beta_{R2\_cn,\,ct}\right) e^{\left(-E_a/kT\right)} \quad (5)$$

$$\log(R_{ch}) = (\beta_{R1\_ch} log(b) + \beta_{R2\_ch}) e^{\left(-E_a/kT\right)} \quad (6)$$

For cnidarians and ctenophores, these relationships were based on equivalent spherical diameter (ESD), which are calculated from carbon biomass of individual organisms (Equation 7; Pitt et al., 2013).

$$\log(ESD) = \beta_{ESD1} \log(b) + \beta_{ESD2} \quad (7)$$

For tunicates, similar to *CR*, we used the experimental literature to derive an allometric relationship between respiration rate and carbon biomass (Equation 6; see Table S2). In the case that respiration rate exceeded the amount of assimilated carbon, respiration was reduced such that production (*P*; assimilated ingestion minus respiration) would never be below zero.

For the temperature scaling, we used the Arrhenius equation with an activation energy (*Ea*) of 0.65 eV (Brown et al., 2004), which corresponds to a Q_{10} scaling of 2.26. In place of in situ temperature, we used SST multiplied by a scaling parameter slightly <1 (c_T) to account for the fact that deeper layers of the euphotic zone are, on average, slightly cooler than the surface. This scaling parameter range was calculated from the depth range in which the GZ organisms were found, according to the JeDI database, and was also subject to selection under the MC procedure (see Table 1). GZ production (*P*) was routed to reproductive losses (*RL*), exudation (*E*), predation (*Pr*), and non-predation mortality (*M*). These fractions routed to *RL*, *E*, and *Pr* (f_{RL}, f_E, and f_{Pr}) were under selection in the MC procedure, with the residual *P* going to *M*. If the sum of the

routing fractions exceeded 1, f_{RL} was first reduced, followed by f_{Pr}. Since the model operates under steady state assumptions, the additional buildup of biomass was not considered. Thus, *RL* in this model only reflects the loss to dissolved organic carbon (DOC) from gamete production, which is likely dependent on reproductive strategies (highly variable in GZ; Boero et al., 2008). Hansson and Norrman (1995) found that reproductive losses were nearly negligible in the moon jelly *Aurelia aurita*. Therefore, we set the initial f_{RL} values in the MC to 0.8–0.16 for ctenophores and tunicates and 0–0.8 for cnidarians.

Exudation (*E*) loss represents mucus production, which occurs mostly during feeding. This can be as high as 40–50% of all C or N released by the organism (Pitt et al., 2009). Though it is sometimes considered a mass- and temperature-independent rate (Condon et al., 2010; Hansson & Norrman, 1995), given that production of mucus is a physiological process, we chose to represent it as production dependent. For the parameter values, since dissolved organic nitrogen production can be 2–3 times higher in ctenophores than scyphozoans (Condon et al., 2010), initial f_E values ranged from 0.15 to 0.45 for ctenophores and 0 to 0.2 for cnidarians. Lastly, since little is known about exudation loss in pelagic tunicates, considering that they feed using mucous meshes, f_E was set to a moderately high range (0.1–0.4).

Predation rates (*Pr*) on GZ by higher trophic levels is a poorly constrained term, largely due to the difficulty in accurately estimating predation rates of soft-bodied, watery organisms that are digested very quickly in predators' guts (Arai, 2005). Previous notions of GZ as trophic dead ends are being challenged, as new methodologies show the importance of GZ in marine food webs (Hays et al., 2018). However, robust estimates of predation rates on GZ are still relatively rare.

As a starting point, we chose to use outputs from Ecopath ecosystem models that explicitly included GZ as an ecosystem component (e.g., Ruzicka et al., 2012). Ecopath models use ecotrophic efficiency (*EE*, unitless), to indicate the amount of production transferred from each trophic level to higher trophic levels via predation (Pauly et al., 2009). Using 30 Ecopath models from 20 ecosystems that explicitly modeled GZ (Aydin et al., 2007; Chiaverano et al., 2018; Mackinson & Daskalov, 2007; Okey & Mahmoudi, 2002; Pauly et al., 2009; Robinson et al., 2015; Ruzicka et al., 2012, 2020), we calculated an average *EE* value of 0.45. This suggests that nearly half of all GZ production is consumed by higher trophic level predators (excluding parasitism by lower trophic levels). In most of the Ecopath models, different groups of GZ were modeled as one generic "jellyfish" group (Pauly et al., 2009), though six models separated GZ into two or more groups (Aydin et al., 2007; Chiaverano et al., 2018; Robinson et al., 2015; Ruzicka et al., 2012, 2020). For the models that separated GZ in multiple groups, individual *EE* values ranged from near zero for sea nettles (*Chrysaora* spp.) and large scyphozoans to over 0.9 for small jellies and filter feeders (e.g., Chiaverano et al., 2018). Thus, in our model, we set the initial f_{Pr} values in the MC to range from 0.2 to 0.55 for cnidarians, 0.4 to 0.9 for ctenophores, and 0.25 to 0.55 for tunicates. We aimed for a total GZ *Pr/P* ratio of 0.45, consistent with the mean Ecopath *EE* value.

2.2.3. Export to Depth Submodel

The second component of the model calculates the depth attenuation of gelatinous-mediated carbon exported out of the surface ocean. This carbon pool includes dead or decaying carcasses and fecal matter. As described in section 2.2.2, fecal pellets are produced by material that is consumed but not assimilated, resulting in the egestion flux *Eg* (Equation 2). Falling carcasses result from assimilated carbon that is not respired, exuded, lost during reproductive processes, or consumed by predators, resulting in the non-predatory mortality flux *M* in Equation 1. These fluxes serve as inputs to an export model which calculates the contribution of GZ to carbon export over 1-D columns on the 1° grid of biomass and GZ production estimates. The cumulative biomass of sinking material is calculated over a year, assuming no net accumulation or loss over that time scale (i.e., $dB/dt = 0$ in Equation 1). We then use the sinking speed and temperature-dependent remineralization equation developed by Lebrato et al. (2011, eq. 9), which used a single first-order kinetic decay constant parameterized for GZ-associated sinking material. Ocean temperatures for this component were obtained from WOA13v2.

POC production from the bioenergetics model were "released" at 20, 20, and 50 m for export originating from cnidarians, ctenophores, and tunicates, respectively. These depths were chosen after evaluation from the average depths of different GZ living biomass within the JeDI database; salps tended to be found at much deeper depths than cnidarians and ctenophores, and thus, their release depth was

greater. For the grid cells that had a maximum depth of 30 m or less, the sinking biomass was released at the surface. For the grid cells with a maximum depth between 30 and 60 m, sinking biomass was released at intermediate depths (10, 10, and 25 m for cnidarians, ctenophores, and tunicates, respectively).

A range of sinking rates for GZ carcasses was used: 1,000–1,200, 800–1,000, and 800–1,200 m d^{-1} for cnidarians, ctenophores, and tunicates, respectively (see Table S3). These values were derived from Lebrato, Mendes, et al. (2013), which found sinking rates of 1,000–1,100 m d^{-1} for scyphozoan cnidarians (though *Periphylla* sank at >1,500 m d^{-1}), 400–600 m d^{-1} for whole ctenophores, 1,100–1,500 m d^{-1} for partial ctenophores, and 800–1,700 m d^{-1} for salps. While considerable uncertainty exists in the sinking speeds of gelatinous carcasses, as a first step, we chose a range of values for this model that reflected the low to middle range of sinking speeds published by Lebrato, Mendes, et al. (2013).

Fecal matter tends to sink slower, though reported sinking rates for salp fecal pellets range from <80 to >2,000 m d^{-1} (Caron et al., 1989; Lebrato, Mendes, et al., 2013; Yoon et al., 2001); the value range we used was 100–1,200 m d^{-1}. Rates of sinking cnidarian and ctenophore fecal matter are unknown, so we used generic values for sinking POC instead (100 m d^{-1}; Turner, 2015). To reduce the computational cost of the model, only discrete sinking rates were implemented where ranges were reported (Table S3).

Export flux values past 100 m, past 1,000 m, and reaching the seafloor were extracted for each 1° grid cell. Global flux estimates were then derived in a manner analogous to the biomass estimates: grid cells were binned by biome, the (arithmetic) mean was calculated, and a global estimate was derived from the area-weighted sum of the fluxes across the biomes. Here we use the arithmetic mean despite non-normality in the distribution of fluxes in order to conserve budgets. Fluxes associated with the slowest, fastest, and mean of all the sinking rates were reported. These flux estimates were validated against values at single-point sites, which were pulled from the literature. In the global domain, estimates of export flux and benthic transfer efficiency (benthic T_{eff}; defined as the proportion of export production at 100 m reaching the seafloor) were compared against literature values (e.g., Dunne et al., 2007; Henson et al., 2012; Laufkötter et al., 2016) and outputs from the COBALT ocean biogeochemistry model (Stock et al., 2014).

2.2.4. Estimating the Uncertainty in the GZ-Mediated Carbon Flux

Significant uncertainty exists regarding the appropriate parameters for a GZ model, as there have been relatively few experiments and an enormous amount of physiological and ecological variability within the GZ. Therefore, we focused efforts on a systematic exploration of parameter space. This consisted of three biomass cases (high, medium, and low), with an ensemble of MC parameter uncertainty estimates associated with each case and a range of sinking speeds for the export model.

We used an MC method to simulate 30,000 random values of 26 different model parameters for the upper ocean bioenergetics model. Parameter values were initialized according to a combination of literature values or best available data and distributed according to a statistical distribution appropriate for the biological process that it described (e.g., Gaussian, log-normal, weighted mean). For a couple parameters (see Table 2), the literature-derived variances were too narrow and did not result in sufficient numbers of accepted parameters; for those, we expanded the variance (while keeping the same mean) for initialization. Full details regarding the mean, variance, and statistical distribution of initialized parameter values are in Table 2.

Candidate models were accepted or rejected based on three criteria.

1. The fraction of grid cells in which respiration needs to be scaled back to match assimilated ingestion (to prevent negative production) cannot exceed 0.4, which roughly represents the fraction of the world's oceans in oligotrophic gyres.
2. The fraction of grid cells in which GZ consumption needs to be scaled back to match prey production (to prevent GZ from consuming more food than was available) cannot exceed 0.7, to allow for both oligotrophic regions and bloom areas.
3. The ratio of respiration to assimilated ingestion has to fall within biological limits, which are 0.2–0.8. Although the respiration fraction may vary by taxa, age, and condition (Costello, 1991; Hansson & Norrman, 1995; Kideys et al., 2004; Kremer & Reeve, 1989; Madin & Purcell, 1992; Uye & Shimauchi, 2005), we thought it would be sensible to keep a single set of broad limits for all taxa.

Table 2
Ranges and Distributions of Parameter Values Used in the MC Simulations

Parameter	Units	Cnidarians	Ctenophores	Tunicates	Distribution
Clearance rate (CR)	L ind.$^{-1}$ d^{-1}	β_{CR1}: 0.81 ± 0.52[a] β_{CR2}: 15.8 ± 1.24		β_{CR1}: 1.2 ± 0.57[b] β_{CR2}: 12.2 ± 0.52	Gaussian
Equivalent spherical diameter (ESD)	cm	β_{ESD1}: 0.33 ± 1.3[c] β_{ESD2}: −0.098 ± 2.9		NA	Gaussian
Respiration	ml O_2 ind.$^{-1}$ h^{-1}	log(R) ~ log (ESD) β_{R1}: 2.59 ± 6.9[d] β_{R2}: 9.22 ± 3.8	 β_{R1}: 2.21 ± 21[e] β_{R2}: 9.44 ± 11	log(R) ~ log (b) β_{R1}: 1.05 ± 2.3[f] β_{R2}: 9.37 ± 1.3	Gaussian
AE (assimilation efficiency)	Unitless	0.32–1.0 (mean: 0.8 ± 0.1)	0.32–1.0 (mean: 0.8 ± 0.1)	0.1–0.9[g] (mean: 0.5 ± 0.2)	Gaussian
c_T (coefficient of temperature)	Unitless	0.924–0.997[h] (mean: 0.986; depths 6–50 m)	0.924–0.997[h] (mean: 0.986; depths 6–50 m)	0.626–0.988[h] (mean: 0.924; depths 18–145 m)	Log-normal
f_E (exudation fraction)	Unitless	0–0.02[i] (mean: 0.1)	0.15–0.45[i] (mean: 0.3)	0.1–0.4[j] (mean: 0.25)	Weighted mean
f_{RL} (reproductive loss fraction)	Unitless	0–0.08[k] (mean: 0.04)	0–0.16[k] (mean: 0.08)	0.08–0.16 (mean: 0.12)	Weighted mean
f_{Pr} (predation fraction)	Unitless	0.2–0.55[l] (mean: 0.375)	0.4–0.85[l] (mean: 0.61)	0.25–0.55[l] (mean: 0.4)	Weighted mean

Note. For each parameter, 30,000 random values were generated following the noted distribution, which were used for model runs. Where necessary, parameter values were converted to standard units. Error terms on the regression coefficients are standard deviations, which were used to generate the range of MC values. Initial tests indicated that these standard deviations were too low for the ESD and respiration allometric scaling parameters and were thus increased to provide a broader range (see footnotes).
[a]Log (CR) = β_{CR1} log(b) + β_{CR2} (Acuña et al., 2011). [b]Log (CR) = β_{CR1} log(b) + β_{CR2} (see Table S1 for references and regression model fit). [c]Conversion between carbon biomass (b, mg C ind.$^{-1}$) and equivalent spherical diameter (ESD, cm): log (ESD) = β_{ESD1} log(b) + β_{ESD2} (Pitt et al., 2013). Standard deviation values for β_{ESD1} and β_{ESD2} were increased by a factor of 10. [d]Log(R) = β_{R1} log (ESD) + β_{R2} (Pitt et al., 2013). Standard deviation values for β_{R1} and β_{R2} were increased by a factor of 10. [e]Log(R) = β_{R1} log (ESD) + β_{R2} (Pitt et al., 2013). Standard deviation values for β_{R1} and β_{R2} were increased by a factor of 10. [f]Log(R) = β_{R1} log(b) + β_{R2} (see Table S2 for model and references). Standard deviation values for β_{R1} and β_{R2} were increased by a factor of 5. [g]For the MC simulations, *AE* was set to a mean of 0.8 for cnidarians and ctenophores (values could not exceed 1), but were lower for tunicates (mean 0.5, though were confined between 0.1 and 0.9). *AE* ranges from 28% to 81% for *Salpa fusiformis* depending on diet (Andersen, 1986) and ~61% for *Cyclosalpa bakeri* (Madin & Purcell, 1992). *S. thompsonii AE*s can range from 0.73 to 0.9 and 0.65 to 0.76 for 13 and 30 mm aggregates, respectively (Pakhomov et al., 2006). [h]Temperatures at depth values were extracted from an average profile for the top 200 m of the world's ocean (from WOA13v2 long-term mean temperatures; Locarnini et al., 2013). The mean depths of upper ocean cnidarians, ctenophores, and chordates (20, 20, and 60 m, respectively) were extracted from the JeDI database (Condon et al., 2015). Log-normal distributions of depths were generated around those means and then associated with an average temperature at depth. c_T represents the ratio of temperature at depth z to temperature at the surface. [i]Exudation fraction was lower for cnidarians than ctenophores (Condon et al., 2010; Costello, 1991; Hansson & Norrman, 1995; Kremer, 1977; Pitt et al., 2009). [j]The tunicate exudation fraction was set to moderately high values due to their feeding with mucous meshes. [k]These values are likely dependent on life history (holoplanktonic or meroplanktonic). *Aurelia aurita* is estimated to contribute 2–4% of ingested C toward reproduction (Hansson & Norrman, 1995). Higher reproductive loss ranges were set for ctenophores and tunicates due to their holoplanktonic and hermaphroditic life history strategies. [l]The predation fraction, f_{Pr}, is equivalent to the ecotrophic efficiency (*EE*) term from the Ecopath models, which represents the rate of biomass production going into higher trophic levels. Predation by other GZ and by lower trophic levels is thus not considered. Ecopath models with GZ reported an *EE* range of 0.45. Here, we maintained an overall mean f_{Pr} of 0.45 over all GZ, but set ctenophore predation to be higher than cnidarians or tunicates due to lack of evidence of ctenophore jelly-falls, which suggests at a greater role for predation versus non-predation mortality.

For the baseline case, 481 cnidarian (1.6%), 1,148 ctenophore (3.8%), and 7,701 tunicate (25%) parameter sets were accepted out of all the MC runs (Figure S2). For the other biomass cases, accepted parameter sets were similar to the baseline: 435/1,028/7,480 (high biomass) and 508/1,267/7,903 (low biomass) for cnidarian/ctenophore/tunicates, and the mean accepted parameter values were also not significantly different (Table S4). For each case, a 100-member ensemble was computed; parameters for the ensemble members were selected at random from the accepted parameter sets. The flux of carbon to depth was calculated for each of these ensemble members under a range of sinking speeds as described in section 2.2.3. Results are reported for the ensemble mean, as well as 95% confidence intervals (CIs), which were calculated using a non-parametric bootstrap method.

3. Results

We revised the global mean estimates of GZ biomass to be 510 Tg C, comprising 290 Tg C cnidarians, 210 Tg C ctenophores, and 11 Tg C pelagic tunicates, which was 13 times higher than L14 due to the modified methodology (Figure 1, Table S5, and Text S1). Estimates of spatial standard deviation (s) was 1.3 Pg C for all GZ and 560 Tg, 1.2 Pg, and 1.5 Pg C for cnidarians, ctenophores, and tunicates, respectively, with the

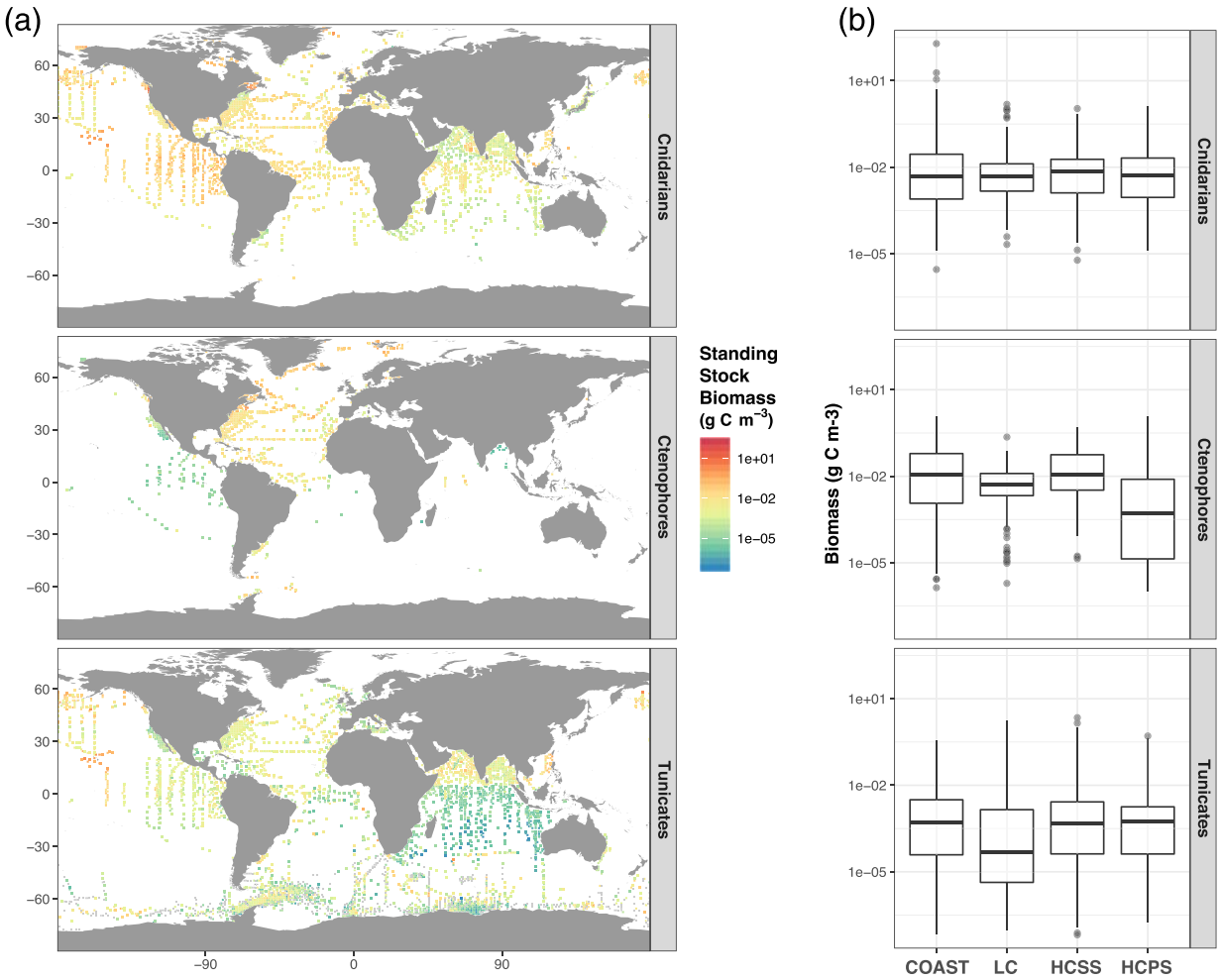

Figure 1. Standing stock biomass of gelatinous zooplankton (GZ). (a) Biomass maps in a global, 1° grid showing the three dominant taxonomic groups: cnidarians, ctenophores, and pelagic tunicates. There are some light gray grid cells (tunicates, Southern Ocean); these indicate true zeros in the data set. (b) Taxa-specific biomass split by biome, which was used to aggregate values for a global estimate. Cnidarians: 2.9E14 g C, ctenophores: 2.1E14 g C, pelagic tunicates: 1.1E13 g C, and combined: 5.1E14 g C. Biome abbreviations are as follows: HCPS, high chlorophyll permanently stratified; HCSS, high chlorophyll seasonally stratified; LC, low chlorophyll. Boxplots show the median, 25% and 75% quartiles (box) and the 1.5 times interquartile range (whiskers), with gray points indicating outliers.

highest spatial variability in the coastal biome (Text S1 and Table S5). These values are contrasted against the standard deviation of the long-term mean, calculated using Condon et al. (2013), which were 180, 120, and 0.6 Tg C for cnidarians, ctenophores, and tunicates, respectively. A detailed description of the biomass calculation is available in Text S1, and differences from previous estimates will be discussed further in section 4.

The biome-based biomass analysis shows an overall similar characteristic biomass for cnidarians and ctenophores, with the exception of ctenophore biomass in the HCPS biome (roughly an order of magnitude lower; Figure 1b and Table S5). For tunicates, their characteristic biomass in the LC biome was roughly half (0.076 mg C m^{-3}) of their biomass in the other high-chlorophyll biomes (0.31–0.34 mg C m^{-3}), but a similar relationship was not evident in the cnidarians and ctenophores. However, spatial variability was higher for cnidarians and ctenophores, particularly in the coastal biome (6.3 and 5.5 mg C m^{-3}, respectively). Indeed, the highest biomass values in the whole data set were cnidarians in the coastal biome, with values exceeding 10 g C m^{-3} (Figure 1b).

Model results show substantial carbon fluxes in the upper 200 m by GZ. From the baseline biomass case, all GZ consumed, on average, 10.9 (95% CIs of ensembles: 9.6–13) Pg C y^{-1}, of which 39%, or 4.2 (3.6–4.9)

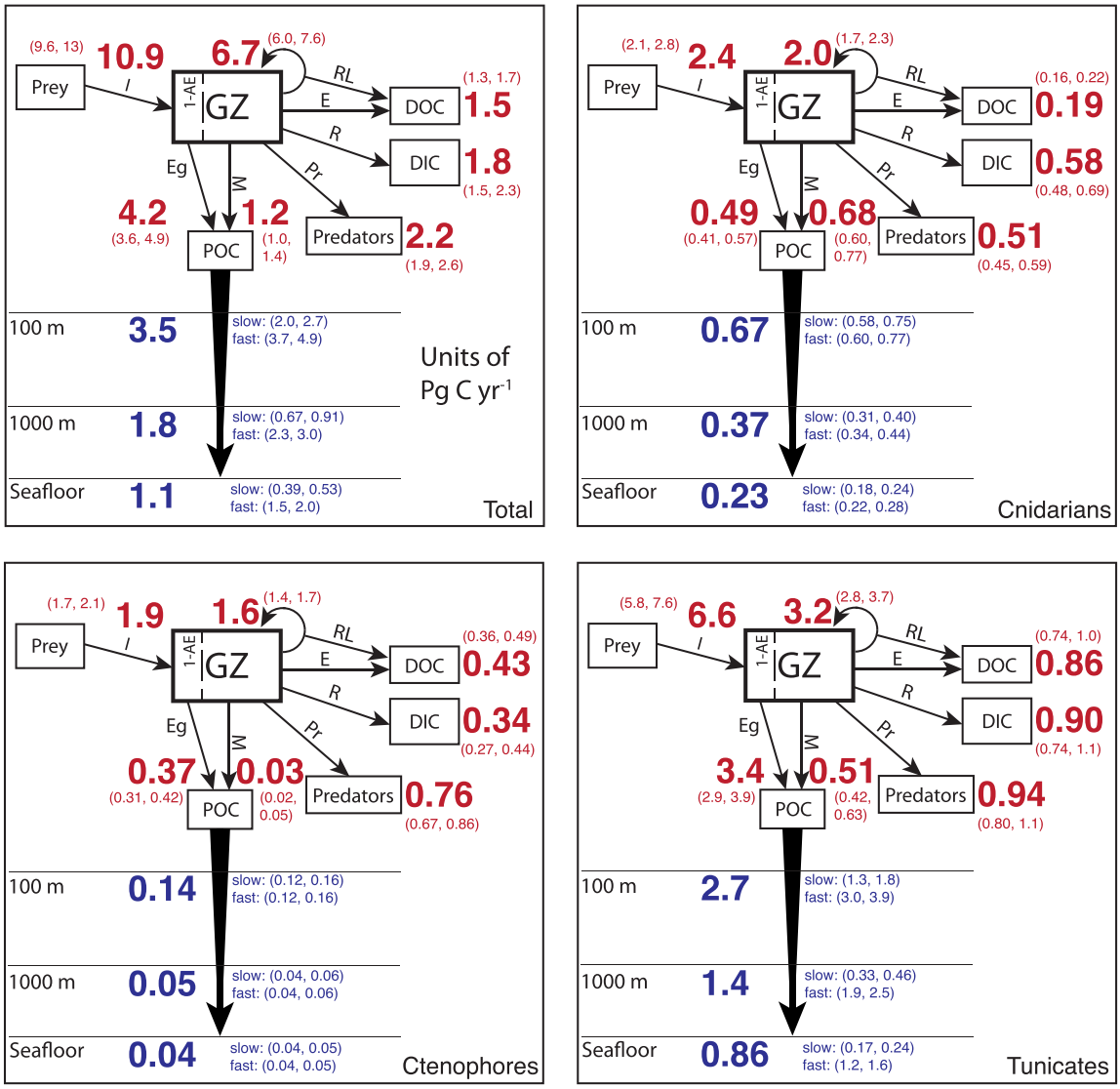

Figure 2. Ensemble mean results for the upper ocean (values in red) and export to depth (values in blue) submodels, shown for all GZ combined, and cnidarians, ctenophores, and pelagic tunicates. Values are given in units of Pg C y^{-1}. Results are only shown for the baseline case. Non-parametric, bootstrapped, 95% confidence intervals (CIs) were calculated from the 100-member ensembles and are shown in the parentheses. For the depth export submodel, CIs were calculated from the slowest and fastest sinking rates at the export depth (100 m), sequestration depth (1,000 m), and seafloor. *AE*, assimilation efficiency; *E*, exudation; *Eg*, egestion; *I*, ingestion; *M*, senescence/mortality; *Pr*, predation; *R*, respiration; *RL*, reproductive losses.

Pg C y^{-1}, was egested as fecal matter and 6.7 (6.0–7.6) Pg C y^{-1} was assimilated. Of the assimilated carbon, 27% (mean: 1.5; CIs: 1.3–1.7 Pg C y^{-1}) was respired, leaving a total GZ production of 4.9 (4.5–5.3) Pg C y^{-1}. The GZ production was then routed to DOC via exudation and reproductive loss (31%, or 1.5 Pg C y^{-1}), predators (45%, or 2.2 Pg C y^{-1}), and finally, 24% to non-predation mortality (mean: 1.2; CIs: 1.0–1.4 Pg C y^{-1}). Total POC production in the top 200 m by GZ was 5.4 (4.6–6.3) Pg C y^{-1}, through fecal matter and carcasses (Figure 2). Results from the other two biomass cases show that the fluxes did not substantially differ from the base case. Top 200 m POC production ranged from 3.7–5.0 Pg C y^{-1} in the low biomass (−1s) case to 5.0–6.8 Pg C y^{-1} in the high biomass (+1s) case (Table S6).

Despite their much lower biomass, the tunicates contributed substantially more to GZ carbon fluxes than cnidarians or ctenophores. For the baseline case, tunicates constituted 47% (2.1–2.6 Pg C y^{-1}) of the total GZ production, whereas cnidarians and ctenophores made up 29% (1.2–1.6 Pg C y^{-1}) and 26% (1.1–1.3 Pg C y^{-1}), respectively. Of the total POC production, tunicates contributed the majority (72%, or

3.3–4.5 Pg C y^{-1}) due to their large fecal pellet production (81% of total). However, tunicate carcass production was lower than that of cnidarians, both as a total flux (0.51 vs. 0.68 Pg C y^{-1}) and as a percentage of their individual production (22% tunicates vs. 48% cnidarians), because more of the tunicate production was routed to other pools. Ctenophores contributed a very modest amount (9%, or 0.37 Pg C y^{-1}) to total fecal matter production and an even smaller fraction (2.5%, or 30 Tg C y^{-1}) to carcasses (Figure 2). For the other biomass cases, results by taxa were fairly similar to the base case (considering that separate MC simulations were done for each case), with cnidarian and ctenophore flux differences fairly minor. For tunicates, flux differences by case were roughly commensurate with the magnitude of biomass changes (Table S6).

The biomass-specific production rates, obtained by dividing production rates by biomass estimates, are an emergent property of the model, and can be compared against laboratory measured specific growth rate. We compiled literature values for GZ daily specific growth, which range from 5 to 66% d^{-1} (mean: 15% d^{-1}) for cnidarians, 6 to 87% d^{-1} (mean: 29% d^{-1}) for ctenophores, and 14 to 71% d^{-1} (mean: 33% d^{-1}) for tunicates (Table S7). In the baseline case of the model, mean daily specific GZ production rates (biome-scaled) were 1.04% d^{-1} for cnidarians, 1.07% d^{-1} for ctenophores, and 11.8% d^{-1} for tunicates. These values fell below the compiled range of GZ specific growth rates for all taxa, though these values represent mean daily specific growth rates averaged over the year. If accounting for a shorter growing season (e.g., 60–90 days), then the modeled values (4.2–6.4% d^{-1} for cnidarians, 4.4–6.5% d^{-1} for ctenophores, and 48–72% d^{-1} for tunicates) fall within the reported range for all three GZ groups, with cnidarians and ctenophores on the lower side and tunicates on the higher side of their respective ranges. This indicates that the model provides a sensible estimate of GZ production.

Production of PO was comprised mainly of fecal matter (78%) and secondarily of carcasses ("jelly-falls"; 22%), though the relative contribution of jelly-falls to total export flux increased with depth due to their faster sinking rates (24–29% at 100 m to 28–35% at the seafloor). In the upper 200 m, sinking POC production totaled 5.4 (CIs: 4.6–6.3) Pg C y^{-1} (Figure 2). Of this POC production, 3.5 (2.0–4.9) Pg C y^{-1} was exported past 100 m (export depth), 1.8 (0.67–3.0) Pg C y^{-1} was exported past 1,000 m (sequestration depth), and 1.1 (0.39–2.0) Pg C y^{-1} reached the seafloor (ranges span the 5% CI of the slow sinkers to the 95% CI of the fast sinkers of all biomass cases; for mean values, see Figure 2). This corresponds to a biome-scaled transfer efficiency (T_{eff}) of roughly 30–61% from 100 to 1,000 m and 20–41% from 100 m to the seafloor. However, when coastal areas (bottom depth <200 m) are ignored, then T_{eff} decreases to 27–58% from 100 to 1,000 m and 13–36% from 100 m to the seafloor; these values are still substantially higher than that of bulk (mostly non-GZ) POC from other estimates (Buesseler et al., 2007; Henson et al., 2012; Weber et al., 2016).

Tunicates contributed the most to export flux, particularly through their fecal pellet flux. On average, the tunicate export flux in the LC biome was not significantly lower than that of the high-chlorophyll biomes, though in the HCPS biome, tunicate fecal pellets flux was nearly 2 times that of the LC biome (Figure 3a). However, the biome-averaged values mask some spatial variation, particularly between the Northern versus Southern Hemispheres. Meridional means reveal the highest seafloor fluxes in the Northern Hemisphere HCSS/HCPS biomes, whereas those same biomes in the Southern Hemisphere had comparatively much lower and variable fluxes (Figure 3b). Further, results resolved on the 1° grid show areas of elevated GZ seafloor fluxes in the North Pacific, eastern equatorial Pacific, and northern Arabian Sea (Figure 3c). These areas were not all associated with high fecal matter flux, which points at an important role for cnidarians and overall jelly-falls for GZ seafloor fluxes as well.

However, high GZ seafloor fluxes do not necessarily imply that those locations are important beyond background levels of non-GZ POC flux, as some of those areas highlighted in Figure 3c also coincide with areas of high net primary productivity (NPP). Instead, an examination of the GZ export ratio (*e*-ratio; Figure 4a) identifies locations where GZ export at 100 m may be elevated beyond background NPP values. Overall, the global mean *e*-ratio for GZ export was 0.070, varying mildly from 0.057 in the LC biome to 0.087 in the HCSS biome. There are some areas where the *e*-ratio was elevated (>0.2), for example, in the South China Sea, but they were overall fairly sparse. Conversely, the GZ benthic T_{eff} (Figure 4b) and its factor difference compared to the benthic T_{eff} in COBALT (Figure 4c) identify potential "hotspots", or areas where GZ may have an elevated impact on POC flux beyond what is currently represented in models. These factor differences range from relatively modest in the LC biome (2.75 times) to moderately high in the coastal and HCPS biomes (4–4.5 times) to very high in the HCSS biome (8.4 times higher than COBALT; Figure 4c).

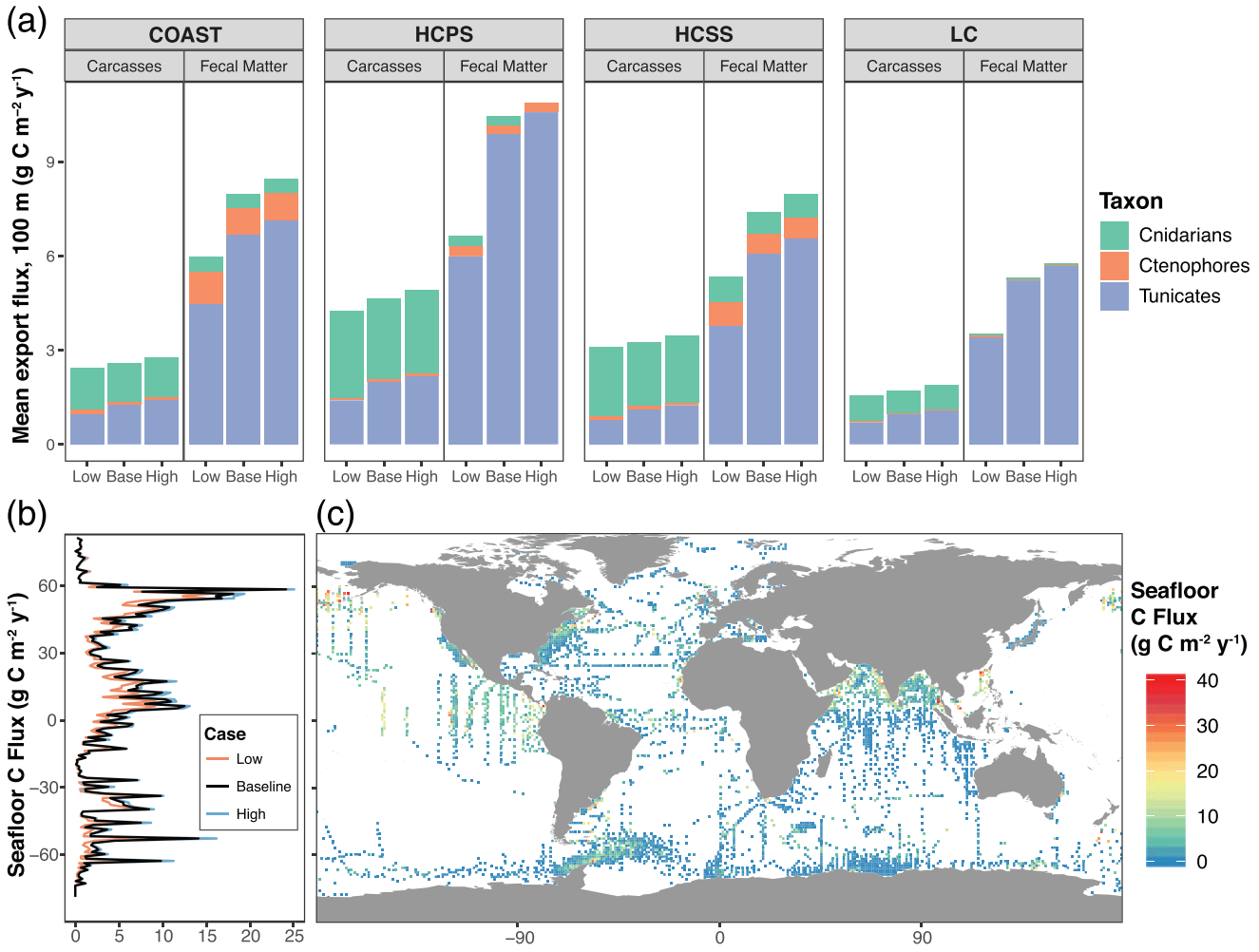

Figure 3. Contributions to seafloor flux. (a) Mean GZ-associated carbon flux associated with carcasses and fecal matter at 100 m for each ocean biome. Fluxes are further partitioned by GZ group. (b) Biome-scaled latitudinal averages and (c) global distribution of seafloor carbon flux (mg C m^{-2} y^{-1}).

Limited observations of GZ-mediated export exist, which allow for some single-point validation of the model, with the caveat that misfits are inevitable when comparing quantities meant to reflect annual mean magnitudes with individual studies. These GZ export observations are primarily from cnidarians in the form of benthic depositions, and tunicates (salps and pyrosomes), which include both benthic depositions and fecal matter from sediment traps. Ctenophores remain an unknown quantity in this respect; to our knowledge, no records of ctenophore benthic depositions or fecal matter exist. Results are given in Table 3 and Figure 5. Compared to observations of tunicate fecal pellets, the model fell within the observational range for nearly all sites: NW Atlantic (Madin et al., 2006; Wiebe et al., 1979), the BATS site in the Sargasso Sea (Stone & Steinberg, 2016), Station M in the NE Pacific (Smith et al., 2014; Wilson et al., 2013), and at various sites in Southern Ocean, including off the WAP (Phillips et al., 2009), Lazarev Sea (Perissinotto & Pakhomov, 1998), and in the Southern Atlantic region (Iversen et al., 2017). However, model results for tunicate fecal pellets were low for another site in the NE Pacific, where the observations only matched some model outlier points (Matsueda et al., 1986), and high compared to Caron et al. (1989) in the subtropical NW Atlantic. While most of the observations were short surveys, there were data from two long-term time series, at Station M and BATS (Smith et al., 2014; Stone & Steinberg, 2016; Wilson et al., 2013), though the BATS data products are also outputs of species-specific models built on top of population time series data (Stone & Steinberg, 2014). At those two sites, the extremes of the model's uncertainty bounds exceeded values from the validation data sets, but the 25–75% quantiles from the model were encompassed within the observational interannual variability.

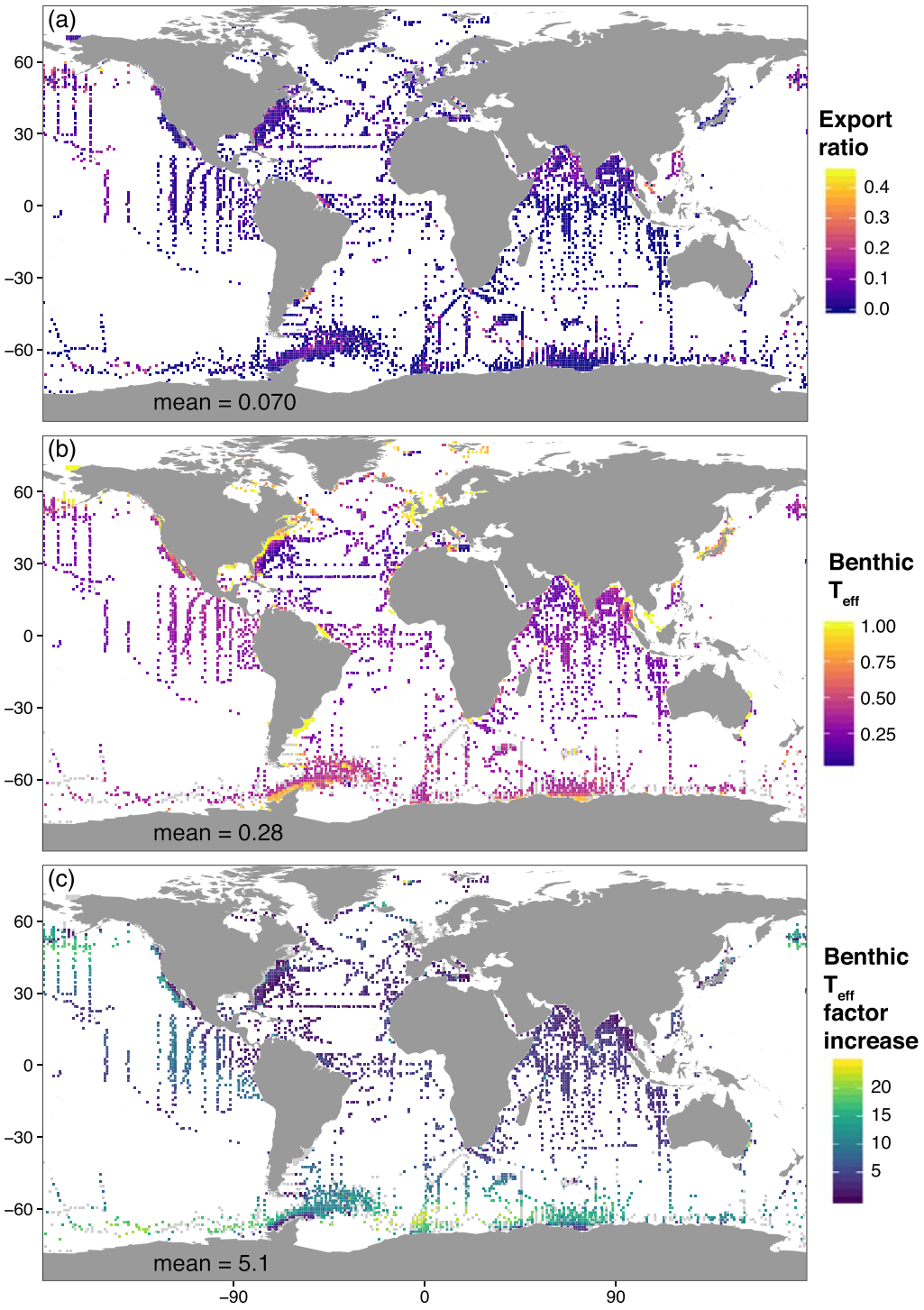

Figure 4. Export ratio (*e*-ratio) and benthic transfer efficiency (T_{eff}) from GZ-associated carbon export and comparisons with the GFDL COBALT v.1 biogeochemical model, showing (a) GZ-associated *e*-ratio, (b) GZ-associated benthic T_{eff}, as defined as the fraction of export flux reaching the seafloor, and (c) the factor increase of benthic T_{eff} for GZ-associated carbon compared to values from the GFDL COBALT v.1 biogeochemical model (for internal consistency). Global mean values are scaled by biomes.

Global Biogeochemical Cycles

10.1029/2020GB006704

Table 3
Comparison Between Observations and the Model Outputs of Gelatinous Carcasses and Fecal Matter at Various Depths

				Observations				Model			
Location	Taxa	Species	Type	Raw value	Data type	Depth range (m)	Transformed value (g C m^{-2} y^{-1})	Loc	Total range (min to max) (g C m^{-2} y^{-1})	95% confidence intervals (g C m^{-2} y^{-1})	Ref.
NW Atlantic	PT	*Salpa aspera*	F	5–91 mg C m^{-2} $night^{-1}$	Rate	300	1.8–33	UO	0.075–58	0.88, 25	Madin et al. (2006)
NW Atlantic	PT	*S. cylindrica, S. maxima, Pegea confoederata*	F	0.01–0.07 mg C m^{-2} d^{-1}	Rate	50	3.–5E-3-0.0255	UO	0.028–56	0.33, 12	Caron et al. (1989)
So. Ocean (West Antarctic P.)	PT	*S. thompsonii*	F	4–20 mg C m^{-2} d^{-1}	Rate	100–500	0.36–1.8	UO	4.0E-3–29	0.12, 10	Phillips et al. (2009)
So. Ocean (Lazarev Sea)	PT	*S. thompsonii*	F	88 mg C m^{-2} d^{-1}	Rate	0–300	7.92	UO	3.5E-3–12	0.15, 5.2	Perissinotto and Pakhomov (1998)
So. Ocean (South Atlantic)	PT	*S. thompsoni*	F	0.1–5.6 mg C m^{-2} d^{-1}	Rate	100–300	0.036–2.1	UO	4.1E-5–1.4	1.7E-3, 0.20	Iversen et al. (2017)
NW Atlantic	PT	*S. aspera*	F	8.5–137 mg C m^{-2} d^{-2}	Rate	>500	3.1–50	S	8.7E-3–41	0.24, 11	Wiebe et al. (1979)
NW Atlantic	PT	*S. aspera*	C	3.6 mg C m^{-2} d^{-1}	Rate	>500	1.31	S	1.6E-3–10	0.036, 2.5	Wiebe et al. (1979)
NE Pacific	PT	Salps	F	8.7 mg C m^{-2} d^{-1}	Rate	4,240	3.17	S	3.6E-8-1.2	1.3E-6, 0.27	Matsueda et al. (1986)
NE Pacific (Station M)	PT	*S. fusiformis*	F	0–4.8 mg C m^{-2} d^{-1}	Rate	3,500–4,000	0–1.75	S	2.3E-4–12	3.1E-3, 1.8	Smith et al. (2014); Wilson et al. (2013)
NE Pacific (Station M)	PT	*S. fusiformis*	C	0–0.5 mg C m^{-2} d^{-1}	Rate	3,500–4,000	0–0.1825	S	2.2E-4–2.5	7.0E-3, 0.38	Smith et al. (2014)
Ivory coast (SE Atlantic)	PT	*P. atlanticum*	C	1–22 g C m^{-2}	SS	900– 1,100	1–22	S	0–2.2	0.020, 0.97	Lebrato and Jones (2009)
NW Mediterranean	PT	*P. atlanticum*	C	0.03–0.07 (max 1.35) mg C m^{-2} mo^{-1}	Rate	319–416	3.6E-4–8.4E-4 (max 0.016)	S	1.2E-3 –4.4	0.038, 1.5	Lebrato, Molinero, et al. (2013)
Tasman Sea	PT	Salps, pyrosomes	C	16 t C km^{-2} y^{-1}	Rate	30–2,500	16	S	4.0E-4–4.6	0.035, 1.5	Henschke et al. (2013)
BATS (Sargasso Sea) (model)	PT	Salps	F	586 ± 1,140 mg C m^{-2} y^{-1}	Rate	200–3,200	0–1.726	S	1.7E-10–13	2.7E-9, 2.8	Stone and Steinberg (2016)
BATS (Sargasso Sea) (model)	PT	Salps	C	23.0 ± 19.5 mg C m^{-2} y^{-1}	Rate	200–3,200	0.0035–0.0425	S	6.8E-5–2.9	5.5E-3, 0.61	Stone and Steinberg (2016)

Table 3
Continued

Location	Taxa	Species	Observations					Model			Ref.
			Type	Raw value	Data type	Depth range (m)	Transformed value (g C m^{-2} y^{-1})	Loc	Total range (min to max) (g C m^{-2} y^{-1})	95% confidence intervals (g C m^{-2} y^{-1})	
Gulf of Oman, Arabian Sea	CN	*Crambionella orsini*	C	1.5–78 g C m^{-2}	SS	300–3,300	1.5–78	S	0–1.6	0, 0.72	Billett et al. (2006)
Lurefjorden, Norway	CN	*Periphylla periphylla*	C	0–72.8 mg C m^{-2} d^{-1}	Rate	447	6.36–11.4	S	3.6E-5 –1.2	2.2E-3, 0.41	Sweetman and Chapman (2015)
Chesapeake Bay	CN	*Chrysaora quinquecirrha*	C	0.17–112.37 mg C m^{-2} y^{-1}	Rate	10–20	1–7*E*-4-0.112	S	4.–E-5-0.53	3.3E-3, 0.26	Sexton et al. (2010)
Sea of Japan	CN	*Nemopilema nomurai*	C	0.2–5.1 ind. 1,000 m^{-2}	SS	146–354	0.562–14.32	S	4.5E-4–3.0	0.020, 1.8	Yamamoto et al. (2008)

Note. Observational data are available as both rates and single event/standing stock observations (SS) ("raw value"), and conversion of the latter to a rate assumes that the single event represents the entirety of the annual carbon flux in that grid cell ("transformed value"). Models' values are given as the absolute range and bootstrapped 95% confidence intervals, incorporating all three biomass cases and each of their 100 ensemble members (see also Figure 5).
Abbreviations: C, carcasses; CN, cnidarians; F, fecal matter; PT, pelagic tunicates; S, seafloor; UO, upper ocean.

In terms of tunicate carcasses, the observations were again encompassed within the model ranges for most sites: the NW Atlantic (Wiebe et al., 1979), the BATS site (Stone & Steinberg, 2016), Station M in the NE Pacific (Smith et al., 2014), and the Ivory Coast (Lebrato & Jones, 2009), though the observational range of the latter site was large and the model only represented the lower bounds. The model was also very low compared to observations from the Tasman Sea (Henschke et al., 2013) and biased high compared to observations from the NW Mediterranean (Lebrato, Molinero, et al., 2013). Overall, the single-point comparisons indicated that the model performed reasonably well in terms of tunicate fecal matter and carcass export.

There are only a few observations of cnidarian carcass depositions (jelly-falls), largely available due to opportunistic sampling in coastal regions. The model results fell within the observational range for the Chesapeake Bay (Sexton et al., 2010) and Sea of Japan (Yamamoto et al., 2008), but had difficulty reproducing the high values from the Gulf of Oman (Billett et al., 2006) and the Norwegian fjords (Sweetman & Chapman, 2015). Since the model uses outputs from the 1° COBALT model, it is understandable and somewhat expected that high fluxes from narrow, deep fjords would be underrepresented. Further, the jelly carcass observations from the Gulf of Oman represent a single mass deposition event and may represent an anomaly compared to mean annual jellyfish fluxes in that region. However, because of the limited number of available observations of cnidarian jelly-falls, we can only say that the model appears to be biased low for these fluxes compared to the observations.

4. Discussion

We developed a data-driven model with uncertainty analysis to estimate potential GZ-mediated carbon flows in the global ocean, which suggests that a GZ biomass standing stock of 510 Tg C can produce 3.7–6.8 Pg C y^{-1} (integrated, top 200 m) of POC, of which 1.6–5.2 Pg C y^{-1} (43–76%) is exported past 100 m, 0.6–3.2 Pg C y^{-1} reaches 1,000 m (16–47%), and 0.4–2.1 Pg C y^{-1} (11–31%) falls to the seafloor. While a data-driven model is subject to some fundamental limitations compared to a coupled ocean biogeochemical model (discussed further below), even values at the low end of the considerable range of outcomes explored in this model are globally significant. Consistent with other efforts (e.g., Lebrato et al., 2019), our model shows that the elevated sinking rates for GZ-associated carbon relative to other forms of organic carbon lead to relatively high transfer efficiencies (T_{eff}) from the surface to the benthos.

Overall, modeled GZ-associated T_{eff} from 100 to 1,000 m were 38–62%, which is lower by 20–35% when compared to Lebrato et al. (2019). This discrepancy is likely due to the overall lower carcass sinking rates in our model compared to data from Lebrato, Mendes, et al. (2013) as well as the separation of sinking carcasses versus fecal pellets in our model. GZ-associated T_{eff} values were higher at high latitudes, due to the temperature-dependent remineralization rates, with latitudinal patterns consistent with that of bulk POC as identified by Marsay et al. (2015) and Weber et al. (2016). However, actual GZ T_{eff} values were still many times greater. Fit to a Martin curve (Martin et al., 1987) using data from 100 m, 1,000 m, and the seafloor, the more efficient GZ-associated carbon export can be represented by a global mean power law attenuation coefficient (b) of 0.18 ± 0.003, which is much lower than the typical, bulk POC value of 0.86 (Buesseler & Boyd, 2009), and regional variations, which span 0.4–2.0 (Buesseler, Lamborg, et al., 2007; Francois et al., 2002; Marsay et al., 2015). This highlights one of the key results of this work, namely, that the relative

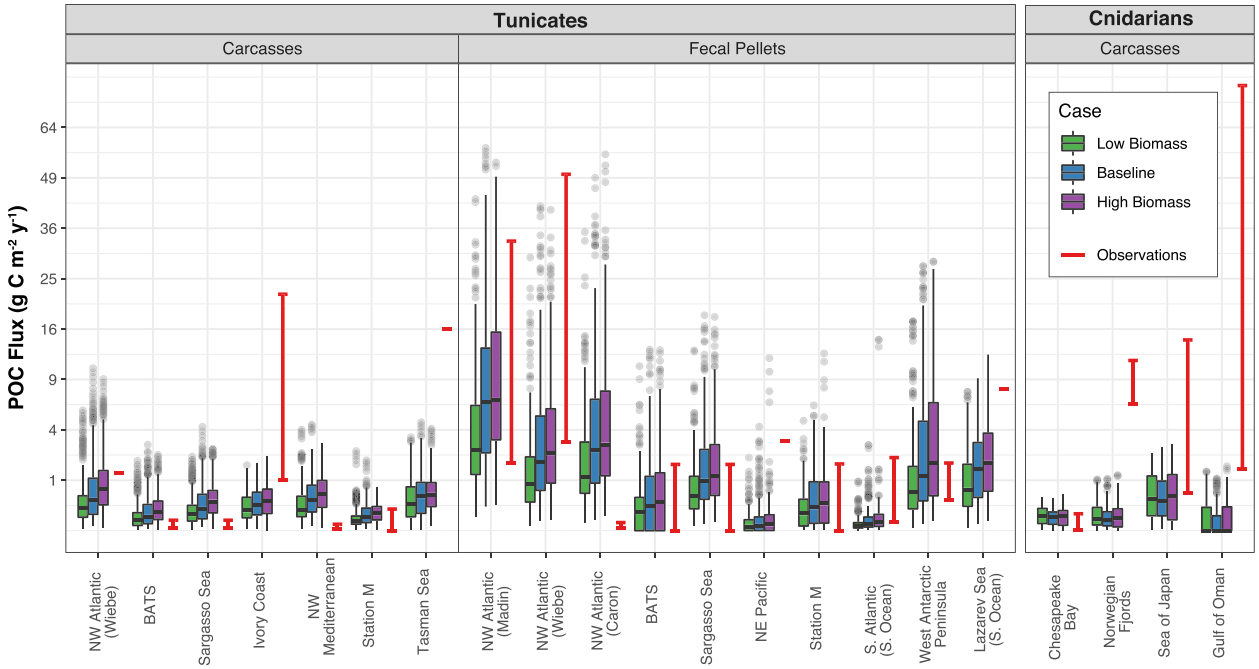

Figure 5. Pointwise comparison of the modeled versus observed POC fluxes for tunicate carcasses, tunicate fecal pellets, and cnidarian carcasses. Model outputs for each case span all ensembles and sinking speeds. For snapshot observations, raw values were converted to fluxes by assuming the observed standing stock represented the entirety of the annual POC flux within that grid cell. References and details are given in Table 3.

importance of GZ-associated carbon flux increases with depth, and the estimated range of 0.4–2.1 Pg C y^{-1} in GZ seafloor flux can be quite significant in fueling benthic food webs.

We validated our model in two ways: first, by comparing specific growth rates from our model against a compilation of literature values for all three GZ groups and second, by comparing export and seafloor flux values at point sites against observations of cnidarian and tunicate carcass depositions and fecal matter flux (Figure 5 and Table 3). The validation efforts showed that broadly, the model agreed with the limited number of direct GZ-mediated export flux observations, particularly with respect to tunicate fluxes. Data from long-term time series are very rare, but at two sites where data and/or data products exist, the 25–75% quantiles of the tunicate fecal pellet flux fell within the observed interannual variability, but the model's outliers were beyond the observational bounds (Smith et al., 2014; Stone & Steinberg, 2016; Wilson et al., 2013). For cnidarians, the model appeared to be biased low compared to the observations, which were all jelly-falls data from coastal sites (Billett et al., 2006; Sexton et al., 2010; Sweetman & Chapman, 2015; Yamamoto et al., 2008), which may be due to a combination of (1) underrepresentation of GZ prey (mesozooplankton) in coastal zones in the 1° resolution COBALT model and (2) uneven sampling of sporadic jelly-fall events that may not be representative of mean cnidarian seafloor fluxes. There are no observations on ctenophore carcass depositions, to our knowledge, though the model also suggested that ctenophore carcass flux would be relatively insignificant (<0.5% of the total export flux). Additional observational data on GZ export flux that span multiple seasons or years, particularly at non-coastal sites, would provide valuable constraints on interannual and spatial variability and would greatly enhance future modeling efforts.

4.1. Model Uncertainties and Constraints

GZ populations are by nature patchy and ephemeral, responding rapidly to changes in the biotic and abiotic environment (Pitt et al., 2014). Many species are only seasonally abundant, with life spans of 3 months or less (Pitt et al., 2014). At dense prey concentrations, GZ can exhibit extremely high growth rates (Table S7), as their high water content and large size enables them to attain much higher clearance rates than crustacean zooplankton with a similar carbon biomass (Acuña et al., 2011). However, during food limitation, the population typically collapses (Purcell & Decker, 2005). These population dynamics naturally make estimates of

GZ biomass, and associated biomass-based modeling, difficult. Furthermore, observational estimates of GZ biomass were historically collected in highly varied ways, such that the data types in the JeDI database range from presence/absence (trawl, plankton net, anecdotal), presence only (remotely operated vehicle, visual survey, museum specimens), categorical (diving, aerial surveys, beach/boat/dock count), and concentration (plankton net, trawl, in situ imagers) (Condon et al., 2012, 2015; updated figure from L14 Appendix S1 in Figure S3). The lack of systematic sampling for GZ is a significant challenge in generating a global data set, but L14 used the concentration data and a subset of the categorical data (e.g., from aerial surveys, Houghton et al., 2006) to compile a "best available" data set for GZ. We supplemented the L14 data set with additional concentration-based data sets from different regions, notably the Southern Ocean (Atkinson et al., 2017), which improved spatial coverage to encompass all major ocean basins.

Even with the additions in the Southern Ocean and elsewhere (section 2.1), GZ observations were only present in 11% of all ocean 1° grid cells (in comparison, mesozooplankton data from the NOAA COPEPOD database were available in 23% of 1° grid cells; Moriarty & O'Brien, 2013). GZ observations also tended to be biased in the Northern Hemisphere and toward coasts. Therefore, we opted for a biome-based approach rooted in the major Banse (1992) biomes to estimate global GZ biomass and modeled fluxes. Biome- or latitudinal-based approaches have been particularly successful in other cases where observational data were sparse or patchy (e.g., Fay & McKinley, 2013; Martiny et al., 2013), as they provide some correction for sampling bias and allow for the broader generalization of sparse data sets. While Banse biomes are coarser than other alternatives (e.g., Longhurst, 1995; Sarmiento et al., 2004), this resolution is consistent with the data sparsity as well as the goals of this contribution in estimating the global contribution of GZ to export flux. Evaluating the different GZ taxa (cnidarians, ctenophores, and tunicates) separately and using the biome-based approach for data extrapolation, combined with the increased spatial coverage, resulted in biomass estimates that were over 10 times higher than the values from L14 (see Text S1 for full discussion).

Increasing spatial coverage in poorly represented ocean regions had a significant impact in refining flux estimates, but due to the sparsity of the data as well as time averaging, the model results are only a coarse view of the magnitude of global GZ carbon cycling. We have explored the implications of biases in the underlying data from extensive testing of the model, as well as running three separate biomass cases. These biomass cases showed that modest variations in biomass (40–60%) at individual grid cells did not substantially change model results for cnidarians and ctenophores (e.g., Figure 3a), which indicates that these groups were largely constrained by bottom-up factors (availability of zooplankton prey). In contrast, tunicate fluxes modulated commensurate with biomass changes, which suggests that they were less bottom-up constrained. Overall, the results suggest that the impact of increases or decreases in GZ biomass depends on which taxa being affected and their food web characteristics.

In addition to biomass, physiological rate parameter uncertainties are the other major source of uncertainty for this model and lie at the heart of future challenges to incorporate prognostic GZ into ocean biogeochemical models. Rates are often measured in the lab, in controlled environments, and with a few species, which may insufficiently represent the range of biological rates within the diverse GZ (cf., Madin & Deibel, 1998). The MC parameter selection procedure was designed to account for and constrain some of this uncertainty and reveal areas in which literature-based parameter values may be inconsistent with a global model formulation. Specifically, initial tests of the MC showed that respiration parameters were too restrictive, and increasing the range of the respiration and ESD allometric scaling parameters (for cnidarians and ctenophores, since R was ESD dependent) was necessary for sufficient simulations to pass the acceptance criteria (see Figure S2 and Table S4). Furthermore, predation on GZ is a highly important and relatively unconstrained factor that was inversely related to jelly-falls. Recent reviews have highlighted the prevalence of GZ as prey (Hays et al., 2018), and here we have used an estimate, based on 30 Ecopath models with explicit GZ, that 45% of all GZ production is consumed by predators. The individual GZ taxa predation levels varied, from 36% to 60% of production (global mean); these values were constrained by other requirements from the MC and the single-point validation. We recognize that there are many unknowns with respect to GZ predation, and other factors that were excluded from consideration (e.g., life history; Henschke et al., 2018), but these global GZ production and predation levels represent initial values upon further work can be done, and the discrepancies between literature and model parameters highlight areas where additional experiments are needed.

Biological rate constraints are one among many for fully evaluating the impact of GZ on the ocean carbon cycle. Others, such as biogeochemical constraints and food web interactions, were beyond the scope of this study but are nonetheless critical. A coupled (i.e., "online") model with GZ integrated into an ocean biogeochemical model could better explore feedbacks, such as between food webs, GZ, and recycled versus exported nutrients, in a manner that could better constrain estimates of carbon export than a data-driven model. In our current study, we have identified a possible range of outcomes and their relative importance to the biological pump.

4.2. Gelatinous Carbon Export

Global estimates of carbon export vary by over threefold, from 4 to 13 Pg C y^{-1} (Dunne et al., 2007; Henson et al., 2011; Laws et al., 2000); our estimates of GZ export at 100 m (1.6–5.2 Pg C y^{-1}) also vary by a factor of 3 and when considering the upper and lower bounds separately, thus comprise 32–40% of total POC export. While some of these GZ-associated fluxes such as salp fecal pellets may already be incorporated into global export flux due to their presence in sediment traps (Gleiber et al., 2012; Wilson et al., 2013), other fluxes such as GZ carcasses are likely not included, due to their large size. Since our estimates of GZ carcass flux at 100 m ranged from 0.48 to 1.2 Pg C y^{-1}, these unaccounted export fluxes, even at the low end of the range, would be globally significant. Current estimates of export flux are typically derived from sediment traps and thorium isotope (^{234}Th) data (Henson et al., 2012; Marsay et al., 2015). Sediment traps have relatively narrow openings, have biases due to the trap boundary layer (Buesseler et al., 2007), and miss nearly all but the smallest GZ carcasses (e.g., doliolids; Takahashi et al., 2013) in their samples (Lebrato et al., 2012). Similarly, since GZ are likely weaker contributors to thorium scavenging in surface waters relative to other sinking particles due to their low surface area to volume ratios, and the GZ C:^{234}Th ratios are not well reflected in sediment traps, their contribution to sinking flux is not well quantified by the thorium approach.

Modeled GZ export fluxes were constrained by primary and secondary production, and the derived GZ-associated *e*-ratio (global mean: 0.07, Figure 4a) is consistent with GZ being a highly significant yet non-dominant contributor to globally averaged surface export fluxes (Earth system models [ESMs] yield global mean export ratios between 0.09 and 0.24; Laufkötter et al., 2016). It was only at deeper depths that the GZ model divergence from ESM-predicted fluxes increases.

Tunicate POC comprised over three quarters of the export flux, with cnidarians comprising most of the remainder, all with substantial geographic variability (Figure 3). These fast-sinking (>1,000 m d^{-1}; Lebrato, Molinero, et al., 2013) materials contribute disproportionately large fluxes as depth increases, such that GZ-mediated seafloor flux at depths >50 m (0.35–2.0 Pg C y^{-1}) could be contributing anywhere from 11% to 140% of benthic POC flux, based on current estimates (1.4–3.2 Pg C y^{-1}; Dunne et al., 2007). Indeed, if considering that the highly sporadic and patchy GZ carcass flux is unlikely to be accounted for in POC flux estimates, the seafloor carcass flux at depths >50 m (0.27–0.5 Pg C y^{-1}) may increase benthic POC flux estimates by 8–35%.

In oceanic regions such as the North Pacific, Southern Ocean, and to a smaller degree, the eastern equatorial Pacific, all high-nitrate low-chlorophyll (HNLC) regions, GZ-mediated benthic flux may be contributing a disproportionate amount relative to other sources of POC (Figure 4c). While there are some cases of highly selective predation by cnidarians and ctenophores (e.g., on fish larvae; Purcell, 1985), GZ as a whole are able to feed at much higher predator-to-prey size ratios than non-GZ (Conley et al., 2018; Hansen et al., 1994). In HNLC regions where iron is limiting for large phytoplankton (diatom) growth, the proliferation of gelatinous filter-feeders that can achieve a 10,000:1 predator-to-prey size ratio may represent one pathway for elevated transfer efficiencies to depth. These areas are likely to be where the impact of GZ on export flux and benthic carbon deposition will be the greatest and where GZ-mediated fluxes could disproportionally benefit benthic feeding crustaceans and fishes (Sweetman et al., 2014).

4.3. Fate of Gelatinous Carbon and the Future Ocean

The results reported here provide a global estimate of the flux of carbon through GZ in the oceans and its fate. GZ production in the upper ocean (3.9–5.8 Pg C y^{-1}) is equivalent to 8–12% of NPP, but their contribution to POC flux increases with depth, such that GZ-POC transfer efficiency is potentially greater than non-GZ POC by fivefold. The GZ carbon reaching the seafloor can, in turn, rapidly leach DOC, feed benthic scavengers, and stimulate the seafloor microbial community (Sweetman et al., 2014; Titelman et al., 2006). A

broad suite of deep-sea organisms scavenge GZ detritus, including fish such as grenadiers and hagfish (Smith et al., 2016; Sweetman et al., 2014), crustaceans such as galatheid crabs, amphipods, and decapod shrimp (Sweetman et al., 2014), and echinoderms including echinoids and ophiuroids (Lebrato & Jones, 2009). As such, episodic jelly-falls are often associated with periodic mass occurrences of benthic organisms (Billett et al., 2006). GZ may be modest components of the upper ocean ecosystem, but for their biomass, their contribution to carbon sequestration through the biological pump and as a food source for deep-sea ecosystems is disproportionately large. Including these processes into global models would have implications for increasing the production and seasonality of benthic meiofauna and their potential responses to climate change (Yool et al., 2017).

Assimilation of global GZ biomass with allometric metabolic scaling equations allows for an improved estimation of gelatinous carbon fluxes in the upper oceans and to depth compared to other efforts that do not take metabolic rates into account (Lebrato et al., 2019). Consistent with assessments that the unique gelatinous body plan maximizes carbon and energy use efficiency (Pitt et al., 2013), our model highlights the outsized role of the relatively modest GZ biomass in funneling globally significant carbon fluxes to the deep sea. However, none of these efforts incorporate the full set of biogeochemical and ecosystem interactions. The marine carbon cycle is often cited as having less uncertainty under climate projections than other systems (i.e., terrestrial ecosystems; Friedlingstein et al., 2014), yet ESMs predict export production to decrease under climate change (−7 to −18% in CMIP5 models by 2100 under the high-emissions scenario; Bopp et al., 2013), with widely varying pathways and drivers (Laufkötter et al., 2016). Furthermore, models have historically overlooked deep-sea biological fluxes, such as jelly-falls, which may add to both the magnitude and variability of climate-carbon feedbacks. These biological processes are short-lived yet significant events that have been challenging to quantify using conventional methods. For example, if observations of jelly-fall events were also incorporated into data sets of benthic oxygen flux (Jahnke, 1996), then biogeochemical modelers could then tune models to be globally consistent with mid-depth oxygen fields while integrating the contributions of GZ biomass.

To better understand the marine biological pump and associated impacts to air-sea fluxes (Kwon et al., 2009), there needs to be additional efforts from both modelers and observationalists on the role of GZ in deep carbon transport. Our study suggests that these fluxes are globally significant and should not be ignored in ocean biogeochemical models. Efforts at including one or more gelatinous functional types in a way that captures their global fluctuations in abundance as well as their relationship to lower trophic level plankton may improve our ability to project future changes to the marine biological pump.

Data Availability Statement

Raw GZ abundance data are available from the Jellyfish Database Initiative (JeDI) repository, hosted on BCO-DMO (https://doi.org/10.1575/1912/7191) (Condon et al., 2015). Gridded, 1°, carbon biomass and numerical density data are available in a Zenodo repository (https://doi.org/10.5281/zenodo.3891704).

Acknowledgments
Many thanks to Su Sponaugle, Kelly Robinson, Jim Ruzicka, Martin Lilley, and Matt Long for helpful discussions. We also thank John Dunne and three anonymous reviewers for comments that improved previous versions of this manuscript. J. Y. L. acknowledges support from NSF (OCE grant 1419987 to R. K. C. and S. Sponaugle) and the NOAA Marine Ecosystem Tipping Points initiative. We also acknowledge support from Biological and Chemical Oceanography Data Management Office (BCO-DMO) for hosting the JeDI data set.

References

Acuña, J. L. (2001). Pelagic tunicates: Why gelatinous? *The American Naturalist*, *158*(1), 100–107.

Acuña, J. L., Lopez-Urrutia, A., & Colin, S. (2011). Faking giants: The evolution of high prey clearance rates in jellyfishes. *Science*, *333*(6049), 1627–1629. https://doi.org/10.1126/Science.1205134

Andersen, V. (1986). Effect of temperature on the filtration rate and percentage of assimilation of Salpa fusiformis Cuvier (Tunicata: Thaliacea). *Hydrobiologia*, *137*(2), 135–140. https://doi.org/10.1007/BF00004209

Arai, M. N. (2005). Predation on pelagic coelenterates: A review. *Journal of the Marine Biological Association of the United Kingdom*, *85*(03), 523–536.

Atkinson, A., Hill, S. L., Pakhomov, E. A., Siegel, V., Anadon, R., Chiba, S., et al. (2017). KRILLBASE: A circumpolar database of Antarctic krill and salp numerical densities, 1926–2016. *Earth System Science Data*, *9*(1), 193–210. https://doi.org/10.5194/essd-9-193-2017

Aydin, K. Y., Gaichas, S., Ortiz, I., Kinzey, D., & Friday, N. (2007). *A comparison of the Bering Sea, Gulf of Alaska, and Aleutian Islands large marine ecosystems through food web modeling* (NOAA Tech. Memo. NMFS-AFSC-178, pp. 1-298). U.S. Department of Commerce, National Oceanic and Atmospheric Administration, National Marine Fisheries Service, Alaska Fisheries Science Center.

Banse, K. (1992). Grazing, temporal changes of phytoplankton concentrations, and the microbial loop in the open sea. In P. G. Falkowski, A. D. Woodhead, & K. Vivirito (Eds.), *Primary productivity and biogeochemical cycles in the sea, Environmental Science Research* (Vol. 43). Boston, MA: Springer. https://doi.org/10.1007/978-1-4899-0762-2_22

Billett, D. S. M., Bett, B. J., Jacobs, C. L., Rouse, I. P., & Wigham, B. D. (2006). Mass deposition of jellyfish in the deep Arabian Sea. *Limnology and Oceanography*, *51*(5), 2077–2083.

Boero, F., Bouillon, J., Gravili, C., Miglietta, M. P., Parsons, T., & Piraino, S. (2008). Gelatinous plankton: Irregularities rule the world (sometimes). *Marine Ecology Progress Series*, *356*, 299–310. https://doi.org/10.3354/meps07368

Bopp, L., Resplandy, L., Orr, J. C., Doney, S. C., Dunne, J. P., Gehlen, M., et al. (2013). Multiple stressors of ocean ecosystems in the 21st century: Projections with CMIP5 models. *Biogeosciences*, *10*(10), 6225–6245. https://doi.org/10.5194/bg-10-6225-2013

Brodeur, R. D., Barcelo, C., Robinson, K. L., Daly, E. A., & Ruzicka, J. J. (2014). Spatial overlap between forage fishes and the large medusa Chrysaora fuscescens in the northern California Current region. *Marine Ecology Progress Series*, *510*, 167–181. https://doi.org/10.3354/meps10810

Brown, J. H., Gillooly, J. F., Allen, A. P., Savage, V. M., & West, G. B. (2004). Toward a metabolic theory of ecology. *Ecology*, *85*(7), 1771–1789. https://doi.org/10.1890/03-9000

Buesseler, K. O., Antia, A. N., Chen, M., Fowler, S. W., Gardner, W. D., Gustafsson, O., et al. (2007). An assessment of the use of sediment traps for estimating upper ocean particle fuxes. *Journal of Marine Research*, *65*(3), 345–416. https://doi.org/10.1357/002224007781567621

Buesseler, K. O., & Boyd, P. W. (2009). Shedding light on processes that control particle export and flux attenuation in the twilight zone of the open ocean. *Limnology and Oceanography*, *54*(4), 1210–1232. https://doi.org/10.4319/lo.2009.54.4.1210

Buesseler, K. O., Lamborg, C. H., Boyd, P. W., Lam, P. J., Trull, T. W., Bidigare, R. R., et al. (2007). Revisiting carbon flux through the ocean's twilight zone. *Science*, *316*(5824), 567–570. https://doi.org/10.1126/science.1137959

Caron, D. a., Madin, L. P., & Cole, J. J. (1989). Composition and degradation of salp fecal pellets: Implications for vertical flux in oceanic environments. *Journal of Marine Research*, *47*(4), 829–850. https://doi.org/10.1357/002224089785076118

Chiaverano, L. M., Robinson, K. L., Tam, J., Ruzicka, J. J., Quiñones, J., Aleksa, K. T., et al. (2018). Evaluating the role of large jellyfish and forage fishes as energy pathways, and their interplay with fisheries, in the Northern Humboldt Current System. *Progress in Oceanography*, *164*, 28–36. https://doi.org/10.1016/j.pocean.2018.04.009

Condon, R. H., Duarte, C. M., Pitt, K. A., Robinson, K. L., Lucas, C. H., Sutherland, K. R., et al. (2013). Recurrent jellyfish blooms are a consequence of global oscillations. *Proceedings of the National Academy of Sciences*, *110*(3), 1000–1005. https://doi.org/10.1073/pnas.1210920110

Condon, R. H., Graham, W. M., Duarte, C. M., Pitt, K. A., Lucas, C. H., Haddock, S. H. D., et al. (2012). Questioning the rise of gelatinous zooplankton in the world's oceans. *Bioscience*, *62*(2), 160–169. https://doi.org/10.1525/Bio.2012.62.2.9

Condon, R. H., Lucas, C. H., Duarte, C. M., Pitt, K. A. (Eds.), (2015). *JeDI: Jellyfish Database Initiative*. Santa Barbara, CA: National Center for Ecological Analysis and Synthesis (NCEAS). https://doi.org/10.1575/1912/7191

Condon, R. H., Steinberg, D. K., & Bronk, D. A. (2010). Production of dissolved organic matter and inorganic nutrients by gelatinous zooplankton in the York River estuary, Chesapeake Bay. *Journal of Plankton Research*, *32*(2), 153–170. https://doi.org/10.1093/plankt/fbp109

Conley, K. R., Lombard, F., & Sutherland, K. R. (2018). Mammoth grazers on the ocean's minuteness: A review of selective feeding using mucous meshes. *Proceedings of the Royal Society B: Biological Sciences*, *285*(1878), 20180056. https://doi.org/10.1098/rspb.2018.0056

Costello, J. (1991). Complete carbon and nitrogen budgets for the hydromedusa Cladonema californicum (Anthomedusa: Cladonemidae). *Marine Biology*, *108*(1), 119–128. https://doi.org/10.1007/BF01313479

de Boyer Montégut, C., Madec, G., Fischer, A. S., Lazar, A., & Iudicone, D. (2004). Mixed layer depth over the global ocean: An examination of profile data and a profile based climatology. *Journal of Geophysical Research*, *109*, C12003. https://doi.org/10.1029/2004JC002378

Dunne, J. P., Sarmiento, J. L., & Gnanadesikan, A. (2007). A synthesis of global particle export from the surface ocean and cycling through the ocean interior and on the seafloor. *Global Biogeochemical Cycles*, *21*, GB4006. https://doi.org/10.1029/2006GB002907

Fay, A. R., & McKinley, G. A. (2013). Global trends in surface ocean pCO2 from in situ data. *Global Biogeochemical Cycles*, *27*, 541–557. https://doi.org/10.1002/gbc.20051

Francois, R., Honjo, S., Krishfield, R., & Manganini, S. (2002). Factors controlling the flux of organic carbon to the bathypelagic zone of the ocean. *Global Biogeochemical Cycles*, *16*(4), 1087. https://doi.org/10.1029/2001gb001722

Friedlingstein, P., Meinshausen, M., Arora, V. K., Jones, C. D., Anav, A., Liddicoat, S. K., & Knutti, R. (2014). Uncertainties in CMIP5 climate projections due to carbon cycle feedbacks. *Journal of Climate*, *27*(2), 511–526. https://doi.org/10.1175/JCLI-D-12-00579.1

Gleiber, M. R., Steinberg, D. K., & Ducklow, H. W. (2012). Time series of vertical flux of zooplankton fecal pellets on the continental shelf of the Western Antarctic Peninsula. *Marine Ecology Progress Series*, *471*, 23–36. https://doi.org/10.3354/meps10021

Hagadorn, J. W., Dott, R. H., & Damrow, D. (2002). Stranded on a Late Cambrian shoreline: Medusae from central Wisconsin. *Geology*, *30*(2), 147–150. https://doi.org/10.1130/0091-7613(2002)030<0147:SOALCS>2.0.CO;2

Hansen, B., Bjørnsen, P. K., & Hansen, P. J. (1994). The size ratio between planktonic predators and their prey. *Limnology and Oceanography*, *39*(2), 395–403. https://doi.org/10.4319/lo.1994.39.2.0395

Hansson, L. J., & Norrman, B. (1995). Release of dissolved organic carbon (DOC) by the scyphozoan jellyfish *Aurelia aurita* and its potential influence on the production of planktic bacteria. *Marine Biology*, *121*(3), 527–532.

Hays, G. C., Doyle, T. K., & Houghton, J. D. R. (2018). A paradigm shift in the trophic importance of jellyfish? *Trends in Ecology & Evolution*, *33*(11), 874–884. https://doi.org/10.1016/j.tree.2018.09.001

Henschke, N., Bowden, D. A., Everett, J. D., Holmes, S. P., Kloser, R. J., Lee, R. W., & Suthers, I. M. (2013). Salp-falls in the Tasman Sea: A major food input to deep-sea benthos. *Marine Ecology Progress Series*, *491*, 165–175. https://doi.org/10.3354/meps10450

Henschke, N., Stock, C. A., & Sarmiento, J. L. (2018). Modeling population dynamics of scyphozoan jellyfish (Aurelia spp.) in the Gulf of Mexico. *Marine Ecology Progress Series*, *591*, 167–183. https://doi.org/10.3354/meps12255

Henson, S. A., Sanders, R., & Madsen, E. (2012). Global patterns in efficiency of particulate organic carbon export and transfer to the deep ocean. *Global Biogeochemical Cycles*, *26*, GB1028. https://doi.org/10.1029/2011GB004099

Henson, S. A., Sanders, R., Madsen, E., Morris, P. J., le Moigne, F., & Quartly, G. D. (2011). A reduced estimate of the strength of the ocean's biological carbon pump. *Geophysical Research Letters*, *38*, L04606. https://doi.org/10.1029/2011GL046735

Heymans, J. J., & Baird, D. (2000). Network analysis of the Northern Benguela ecosystem by means of NETWRK and ECOPATH. *Ecological Modelling*, *131*(2–3), 97–119. https://doi.org/10.1016/S0304-3800(00)00275-1

Houghton, J. D. R., Doyle, T. K., Davenport, J., & Hays, G. C. (2006). Developing a simple, rapid method for identifying and monitoring jellyfish aggregations from the air. *Marine Ecology Progress Series*, *314*, 159–170. https://doi.org/10.3354/meps314159

Iversen, M. H., Pakhomov, E. A., Hunt, B. P. V., van der Jagt, H., Wolf-Gladrow, D., & Klaas, C. (2017). Sinkers or floaters? Contribution from salp pellets to the export flux during a large bloom event in the Southern Ocean. *Deep-Sea Research Part II: Topical Studies in Oceanography*, *138*, 116–125. https://doi.org/10.1016/j.dsr2.2016.12.004

Jahnke, R. A. (1996). The global ocean flux of particulate organic carbon: Areal distribution and magnitude. *Global Biogeochemical Cycles*, *10*(1), 71–88. https://doi.org/10.1029/95GB03525

Kideys, A. E., Finenko, G. A., Anninsky, B. E., Shiganova, T. A., Roohi, A., Tabari, M. R., et al. (2004). Physiological characteristics of the ctenophore Beroe ovata in Caspian Sea water. *Marine Ecology Progress Series*, *266*, 111–121. https://doi.org/10.3354/meps266111

Kremer, P. (1977). Respiration and excretion by the ctenophore Mnepiopsis leidyi. *Marine Biology*, *44*(1), 43–50. https://doi.org/10.1007/BF00386903

Kremer, P., & Reeve, M. R. (1989). Growth dynamics of a ctenophore (Mnemiopsis) in relation to variable food supply. II. Carbon budgets and growth model. *Journal of Plankton Research*, *11*(3), 553–574.

Kwon, E. Y., Primeau, F., & Sarmiento, J. L. (2009). The impact of remineralization depth on the air-sea carbon balance. *Nature Geoscience*, *2*(9), 630–635. https://doi.org/10.1038/ngeo612

Laufkötter, C., Vogt, M., Gruber, N., Aita-Noguchi, M., Aumont, O., Bopp, L., et al. (2016). Projected decreases in future marine export production : The role of the carbon flux through the upper ocean ecosystem. *Biogeosciences*, *12*(4), 3731–3824. https://doi.org/10.5194/bgd-12-3731-2015

Laws, E. A., Falkowski, P. G., Smith, W. O., Ducklow, H., & McCarthy, J. J. (2000). Temperature effects on export production in the open ocean. *Global Biogeochemical Cycles*, *14*(4), 1231–1246.

Lebrato, M., & Jones, D. O. B. (2009). Mass deposition event of Pyrosoma atlanticum carcasses off Ivory Coast (West Africa). *Limnology and Oceanography*, *54*(4), 1197–1209. https://doi.org/10.4319/Lo.2009.54.4.1197

Lebrato, M., Mendes, P. J., Steinberg, D. K., Cartes, J. E., Jones, B. M., Birsa, L. M., et al. (2013). Jelly biomass sinking speed reveals a fast carbon export mechanism. *Limnology and Oceanography*, *58*(3), 1113–1122. https://doi.org/10.4319/lo.2013.58.3.1113

Lebrato, M., Molinero, J. C., Cartes, J. E., Lloris, D., Melin, F., & Beni-Casadella, L. (2013). Sinking jelly-carbon unveils potential environmental variability along a continental margin. *PLoS ONE*, *8*(12), e82070. https://doi.org/10.1371/journal.pone.0082070

Lebrato, M., Pahlow, M., Frost, J. R., Küter, M., Mendes, P. D. J., Molinero, J. C., & Oschlies, A. (2019). Sinking of gelatinous zooplankton biomass increases deep carbon transfer efficiency globally. *Global Biogeochemical Cycles*, *33*, 1764–1783. https://doi.org/10.1029/2019GB006265

Lebrato, M., Pahlow, M., Oschlies, A., Pitt, K. A., Jones, D. O. B., Molinero, J. C., & Condon, R. H. (2011). Depth attenuation of organic matter export associated with jelly falls. *Limnology and Oceanography*, *56*(5), 1917–1928. https://doi.org/10.4319/lo.2011.56.5.1917

Lebrato, M., Pitt, K. A., Sweetman, A. K., Jones, D. O. B., Cartes, J. E., Oschlies, A., et al. (2012). Jelly-falls historic and recent observations: A review to drive future research directions. *Hydrobiologia*, *690*(1), 227–245. https://doi.org/10.1007/s10750-012-1046-8

Lilley, M. K. S., Beggs, S. E., Doyle, T. K., Hobson, V. J., Stromberg, K. H. P., & Hays, G. C. (2011). Global patterns of epipelagic gelatinous zooplankton biomass. *Marine Biology*, *158*(11), 2429–2436. https://doi.org/10.1007/s00227-011-1744-1

Locarnini, R. A., Mishonov, A. V., Antonov, J. I., Boyer, T. P., Garcia, H. E., Baranova, O. K., et al. (2013). In S. Levitus (Ed.), *World Ocean Atlas 2013, Volume 1: Temperature*. NOAA Atlas NESDIS.

Longhurst, A. (1995). Seasonal cycles of pelagic production and consumption. *Progress in Oceanography*, *36*(2), 77–167. https://doi.org/10.1016/0079-6611(95)00015-1

Lucas, C. H., & Dawson, M. N. (2014). What are jellyfishes and Thaliaceans and why do they bloom? In K. A. Pitt, & C. H. Lucas (Eds.), *Jellyfish blooms* (pp. 9–44). Netherlands: Springer. https://doi.org/10.1007/978-94-007-7015-7_2

Lucas, C. H., Jones, D. O. B., Hollyhead, C. J., Condon, R. H., Duarte, C. M., Graham, W. M., et al. (2014). Gelatinous zooplankton biomass in the global oceans: Geographic variation and environmental drivers. *Global Ecology and Biogeography*, *23*(7), 701–714. https://doi.org/10.1111/geb.12169

Lucas, C. H., Pitt, K. A., Purcell, J. E., Lebrato, M., & Condon, R. H. (2011). What's in a jellyfish? Proximate and elemental composition and biometric relationships for use in biogeochemical studies. *Ecology*, *92*(8), 1704. https://doi.org/10.1890/11-0302.1

Mackinson, S., & Daskalov, G. (2007). *An ecosystem model of the North Sea to support an ecosystem approach to fisheries management: Description and parameterisation, Cefas Science Series Technical Report*. (Vol. *142*, p. 196). Lowestoft, UK: Cefas.

Madin, L. P., & Deibel, D. (1998). Feeding and energetics of Thaliacea. In Q. Bone (Ed.), *The biology of pelagic tunicates* (pp. 81–103). New York, USA: Oxford University Press.

Madin, L. P., Kremer, P., Wiebe, P. H., Purcell, J. E., Horgan, E. H., & Nemazie, D. A. (2006). Periodic swarms of the salp Salpa aspera in the Slope Water off the NE United States: Biovolume, vertical migration, grazing, and vertical flux. *Deep-Sea Research Part I—Oceanographic Research Papers*, *53*(5), 804–819. https://doi.org/10.1016/j.dsr.2005.12.018

Madin, L. P., & Purcell, J. E. (1992). Feeding, metabolism, and growth of *Cyclosalpa bakeri* in the subarctic Pacific. *Limnology and Oceanography*, *37*(6), 1236–1251. https://doi.org/10.4319/lo.1992.37.6.1236

Marsay, C. M., Sanders, R. J., Henson, S. A., Pabortsava, K., Achterberg, E. P., & Lampitt, R. S. (2015). Attenuation of sinking particulate organic carbon flux through the mesopelagic ocean. *Proceedings of the National Academy of Sciences*, *112*(4), 1089–1094. https://doi.org/10.1073/pnas.1415311112

Martin, J. H., Knauer, G. A., Karl, D. M., & Broenkow, W. W. (1987). VERTEX: Carbon cycling in the northeast Pacific. *Deep Sea Research Part A. Oceanographic Research Papers*, *34*(2), 267–285.

Martiny, A. C., Pham, C. T. A., Primeau, F. W., Vrugt, J. A., Moore, J. K., Levin, S. A., & Lomas, M. W. (2013). Strong latitudinal patterns in the elemental ratios of marine plankton and organic matter. *Nature Geoscience*, *6*(4), 279–283. https://doi.org/10.1038/ngeo1757

Matsueda, H., Handa, N., Inoue, I., & Takano, H. (1986). Ecological significance of salp fecal pellets collected by sediment traps in the eastern North Pacific. *Marine Biology*, *91*(3), 421–431. https://doi.org/10.1007/BF00428636

Moriarty, R., & O'Brien, T. D. (2013). Distribution of mesozooplankton biomass in the global ocean. *Earth System Science Data*, *5*(1), 45–55. https://doi.org/10.5194/essd-5-45-2013

Okey, T. A., & Mahmoudi, B. (2002). *An ecosystem model of the West Florida shelf for use in fisheries management and ecological research: Volume II. Model construction*. St. Petersburg, FL: Florida Marine Research Institute.

Pakhomov, E. A., Dubischar, C. D., Strass, V., Brichta, M., & Bathmann, U. V. (2006). The tunicate *Salpa thompsoni* ecology in the Southern Ocean. I. Distribution, biomass, demography and feeding ecophysiology. *Marine Biology*, *149*(3), 609–623.

Pauly, D., Graham, W., Libralato, S., Morissette, L., & Deng Palomares, M. (2009). Jellyfish in ecosystems, online databases, and ecosystem models. *Hydrobiologia*, *616*(1), 67–85. https://doi.org/10.1007/s10750-008-9583-x

Perissinotto, R., & Pakhomov, E. A. (1998). Contribution of salps to carbon flux of marginal ice zone of the Lazarev Sea, Southern Ocean. *Marine Biology*, *131*(1), 25–32.

Phillips, B., Kremer, P., & Madin, L. P. (2009). Defecation by *Salpa thompsoni* and its contribution to vertical flux in the Southern Ocean. *Marine Biology*, *156*(3), 455–467. https://doi.org/10.1007/s00227-008-1099-4

Pitt, K. A., Budarf, A. C., Browne, J. G., & Condon, R. H. (2014). Bloom and bust: Why do blooms of jellyfish collapse? In *Jellyfish blooms* (pp. 79–103). NewYork: Springer.

Pitt, K. A., Duarte, C. M., Lucas, C. H., Sutherland, K. R., Condon, R. H., Mianzan, H., et al. (2013). Jellyfish body plans provide allometric advantages beyond low carbon content. *PLoS ONE*, *8*(8), e72683. https://doi.org/10.1371/journal.pone.0072683

Pitt, K. A., Welsh, D. T., & Condon, R. H. (2009). Influence of jellyfish blooms on carbon, nitrogen and phosphorus cycling and plankton production. *Hydrobiologia*, *616*(1), 133–149. https://doi.org/10.1007/s10750-008-9584-9

Purcell, J. E. (1985). Predation on fish eggs and larvae by pelagic cnidarians and ctenophores. *Bulletin of Marine Science*, *37*(2), 739–755.

Purcell, J. E. (2012). Jellyfish and ctenophore blooms coincide with human proliferations and environmental perturbations. *Annual Review of Marine Science*, *4*(4), 209–235. https://doi.org/10.1146/Annurev-Marine-120709-142751

Purcell, J. E., & Decker, M. B. (2005). Effects of climate on relative predation by scyphomedusae and ctenophores on copepods in Chesapeake Bay during 1987–2000. *Limnology and Oceanography*, *50*(1), 376–387.

Reynolds, R. W., Rayner, N. A., Smith, T. M., Stokes, D. C., & Wang, W. (2002). An improved in situ and satellite SST analysis for climate. *Journal of Climate*, *15*(13), 1609–1625.

Robinson, K. L., Ruzicka, J. J., Hernandez, F. J., Graham, W. M., Decker, M. B., Brodeur, R. D., & Sutor, M. (2015). Evaluating energy flows through jellyfish and gulf menhaden (*Brevoortia patronus*) and the effects of fishing on the northern Gulf of Mexico ecosystem. *ICES Journal of Marine Science*, *72*(8), 2301–2312. https://doi.org/10.1093/icesjms/fsv088

Ruzicka, J., Brodeur, R. D., Cieciel, K., & Decker, M. B. (2020). Examining the ecological role of jellyfish in the Eastern Bering Sea. *ICES Journal of Marine Science*, *77*(2), 791–802. https://doi.org/10.1093/icesjms/fsz244

Ruzicka, J. J., Brodeur, R. D., Emmett, R. L., Steele, J. H., Zamon, J. E., Morgan, C. A., et al. (2012). Interannual variability in the northern California Current food web structure: Changes in energy flow pathways and the role of forage fish, euphausiids, and jellyfish. *Progress in Oceanography*, *102*, 19–41. https://doi.org/10.1016/j.pocean.2012.02.002

Sarmiento, J. L., Slater, R., Barber, R., Bopp, L., Doney, S. C., Hirst, A. C., et al. (2004). Response of ocean ecosystems to climate warming. *Global Biogeochemical Cycles*, *18*, GB3003. https://doi.org/10.1029/2003GB002134

Sexton, M. A., Hood, R. R., Sarkodee-adoo, J., & Liss, A. M. (2010). Response of *Chrysaora quinquecirrha* medusae to low temperature. *Hydrobiologia*, *645*(1), 125–133. https://doi.org/10.1007/s10750-010-0222-y

Shenker, J. M. (1985). Carbon content of the neritic scyphomedusa *Chrysaora fuscescens*. *Journal of Plankton Research*, *7*(2), 169–173.

Smith, B. E., Ford, M. D., & Link, J. S. (2016). Bloom or bust: Synchrony in jellyfish abundance, fish consumption, benthic scavenger abundance, and environmental drivers across a continental shelf. *Fisheries Oceanography*, *25*(5), 500–514. https://doi.org/10.1111/fog.12168

Smith, K. L. Jr., Sherman, A. D., Huffard, C. L., McGill, P. R., Henthorn, R., von Thun, S., et al. (2014). Large salp bloom export from the upper ocean and benthic community response in the abyssal northeast Pacific: Day to week resolution. *Limnology and Oceanography*, *59*(3), 745–757. https://doi.org/10.4319/lo.2014.59.3.0745

Steinberg, D. K., & Landry, M. R. (2017). Zooplankton and the ocean carbon cycle. *Annual Review of Marine Science*, *9*(1), 413–444. https://doi.org/10.1146/annurev-marine-010814-015924

Steinberg, D. K., Ruck, K. E., Gleiber, M. R., Garzio, L. M., Cope, J. S., Bernard, K. S., et al. (2015). Long-term (1993–2013) changes in macrozooplankton off the Western Antarctic Peninsula. *Deep Sea Research Part I: Oceanographic Research Papers*, *101*, 54–70. https://doi.org/10.1016/j.dsr.2015.02.009

Stock, C. A., Dunne, J. P., & John, J. G. (2014). Global-scale carbon and energy flows through the marine planktonic food web: An analysis with a coupled physical-biological model. *Progress in Oceanography*, *120*, 1–28.

Stone, J. P., & Steinberg, D. K. (2014). Long-term time-series study of salp population dynamics in the Sargasso Sea. *Marine Ecology Progress Series*, *510*, 111–127. https://doi.org/10.3354/meps10985

Stone, J. P., & Steinberg, D. K. (2016). Salp contributions to vertical carbon flux in the Sargasso Sea. *Deep-Sea Research Part I: Oceanographic Research Papers*, *113*, 90–100. https://doi.org/10.1016/j.dsr.2016.04.007

Sutherland, K. R., Madin, L. P., & Stocker, R. (2010). Filtration of submicrometer particles by pelagic tunicates. *Proceedings of the National Academy of Sciences*, *107*(34), 15,129–15,134.

Sweetman, A. K., & Chapman, A. (2011). First observations of jelly-falls at the seafloor in a deep-sea fjord. *Deep-Sea Research Part I: Oceanographic Research Papers*, *58*(12), 1206–1211. https://doi.org/10.1016/j.dsr.2011.08.006

Sweetman, A. K., & Chapman, A. (2015). First assessment of flux rates of jellyfish carcasses (jelly-falls) to the benthos reveals the importance of gelatinous material for biological C-cycling in jellyfish-dominated ecosystems. *Frontiers in Marine Science*, *2*(47). https://doi.org/10.3389/fmars.2015.00047

Sweetman, A. K., Smith, C. R., Dale, T., & Jones, D. O. B. (2014). Rapid scavenging of jellyfish carcasses reveals the importance of gelatinous material to deep-sea food webs. *Proceedings of the Royal Society B: Biological Sciences*, *281*(1796). https://doi.org/10.1098/Rspb.2014.2210

Takahashi, K., Ichikawa, T., Saito, H., Kakehi, S., Sugimoto, Y., Hidaka, K., & Hamasaki, K. (2013). Sapphirinid copepods as predators of doliolids: Their role in doliolid mortality and sinking flux. *Limnology and Oceanography*, *58*(6), 1972–1984. https://doi.org/10.4319/lo.2013.58.6.1972

Titelman, J., Riemann, L., Sørnes, T. A., Nilsen, T., Griekspoor, P., & Båmstedt, U. (2006). Turnover of dead jellyfish: Stimulation and retardation of microbial activity. *Marine Ecology Progress Series*, *325*, 43–58. Retrieved from http://www.scopus.com/inward/record.url?eid=2-s2.0-33,845,401,318&partnerID=40&md5=4278960d7965d4c8d718b7bbdabf3b6d

Turner, J. T. (2015). Zooplankton fecal pellets, marine snow, phytodetritus and the ocean's biological pump. *Progress in Oceanography*, *130*, 205–248. https://doi.org/10.1016/j.pocean.2014.08.005

Uye, S.-I., & Shimauchi, H. (2005). Population biomass, feeding, respiration and growth rates, and carbon budget of the scyphomedusa *Aurelia aurita* in the Inland Sea of Japan. *Journal of Plankton Research*, *27*(3), 237–248.

Vasas, V., Lancelot, C., Rousseau, V., & Jordán, F. (2007). Eutrophication and overfishing in temperate nearshore pelagic food webs: A network perspective. *Marine Ecology Progress Series*, *336*, 1–14. https://doi.org/10.3354/meps336001

Weber, T., Cram, J. A., Leung, S. W., DeVries, T., & Deutsch, C. (2016). Deep ocean nutrients imply large latitudinal variation in particle transfer efficiency. *Proceedings of the National Academy of Sciences*, *113*(31), 8606–8611. https://doi.org/10.1073/pnas.1604414113

Wiebe, P. H., Madin, L. P., Haury, L. R., Harbison, G. R., & Philbin, L. M. (1979). Diel vertical migration by Salpa aspera and its potential for large-scale particulate organic matter transport to the deep-sea. *Marine Biology*, *53*(3), 249–255.

Wilson, S. E., Ruhl, H. A., & Smith Jr, K. L. (2013). Zooplankton fecal pellet flux in the abyssal northeast Pacific: A 15 year time-series study. *Limnology and Oceanography*, *58*(3), 881–892.

Yamamoto, J., Hirose, M., Ohtani, T., Sugimoto, K., Hirase, K., Shimamoto, N., et al. (2008). Transportation of organic matter to the sea floor by carrion falls of the giant jellyfish Nemopilema nomurai in the Sea of Japan. *Marine Biology*, *153*(3), 311–317. https://doi.org/10.1007/s00227-007-0807-9

Yool, A., Martin, A. P., Anderson, T. R., Bett, B. J., Jones, D. O. B., & Ruhl, H. A. (2017). Big in the benthos: Future change of seafloor community biomass in a global, body size-resolved model. *Global Change Biology*, *23*(9), 3554–3566. https://doi.org/10.1111/gcb.13680

Yoon, W., Kim, S., & Han, K. (2001). Morphology and sinking velocities of fecal pellets of copepod, molluscan, euphausiid, and salp taxa in the northeastern tropical Atlantic. *Marine Biology*, *139*(5), 923–928. https://doi.org/10.1007/s002270100630